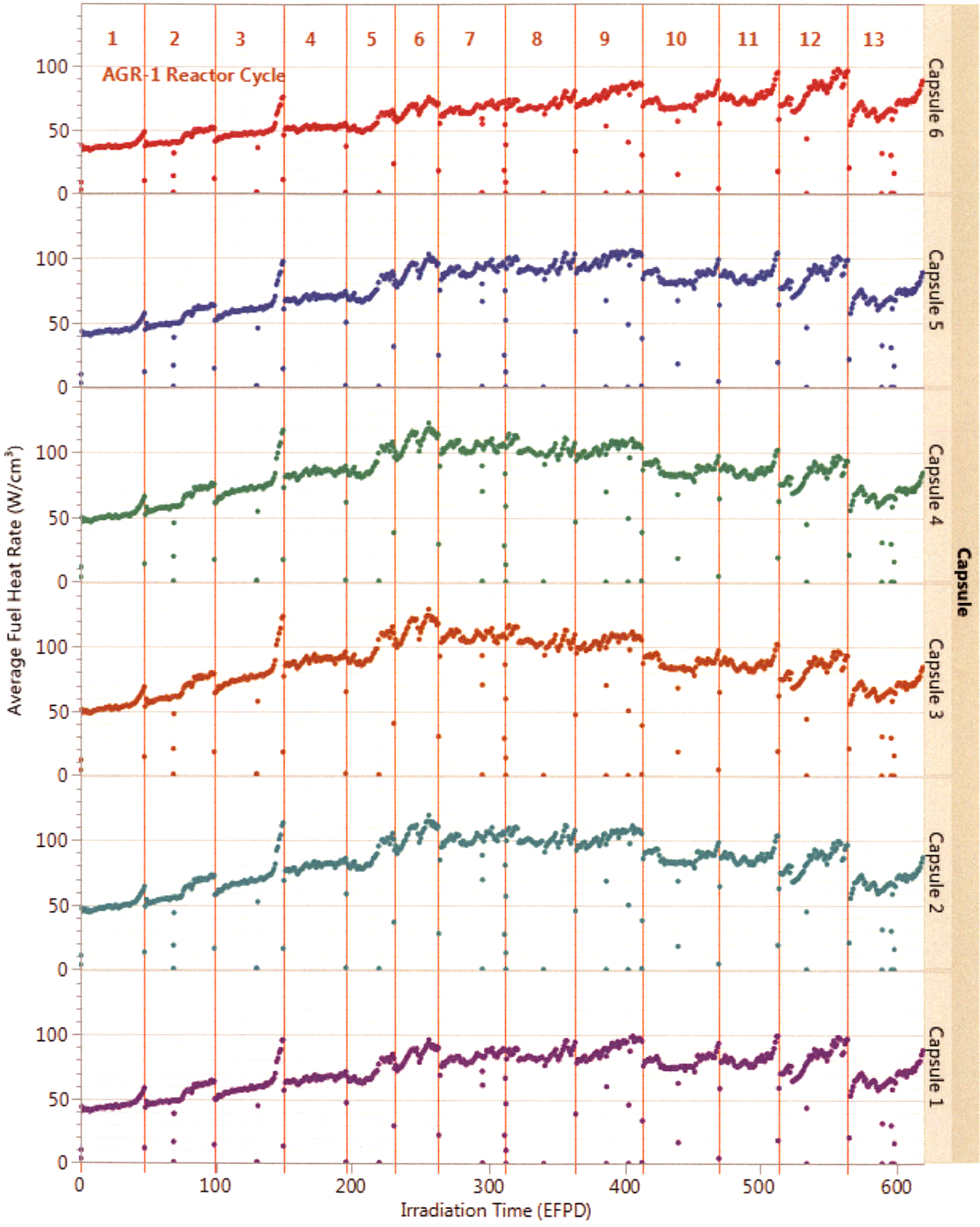

Figure 6-6
AGR-1 capsule average power density versus irradiation time in EFPDs
Courtesy of Idaho National Laboratory and used with permission of Battelle Energy Alliance, LLC

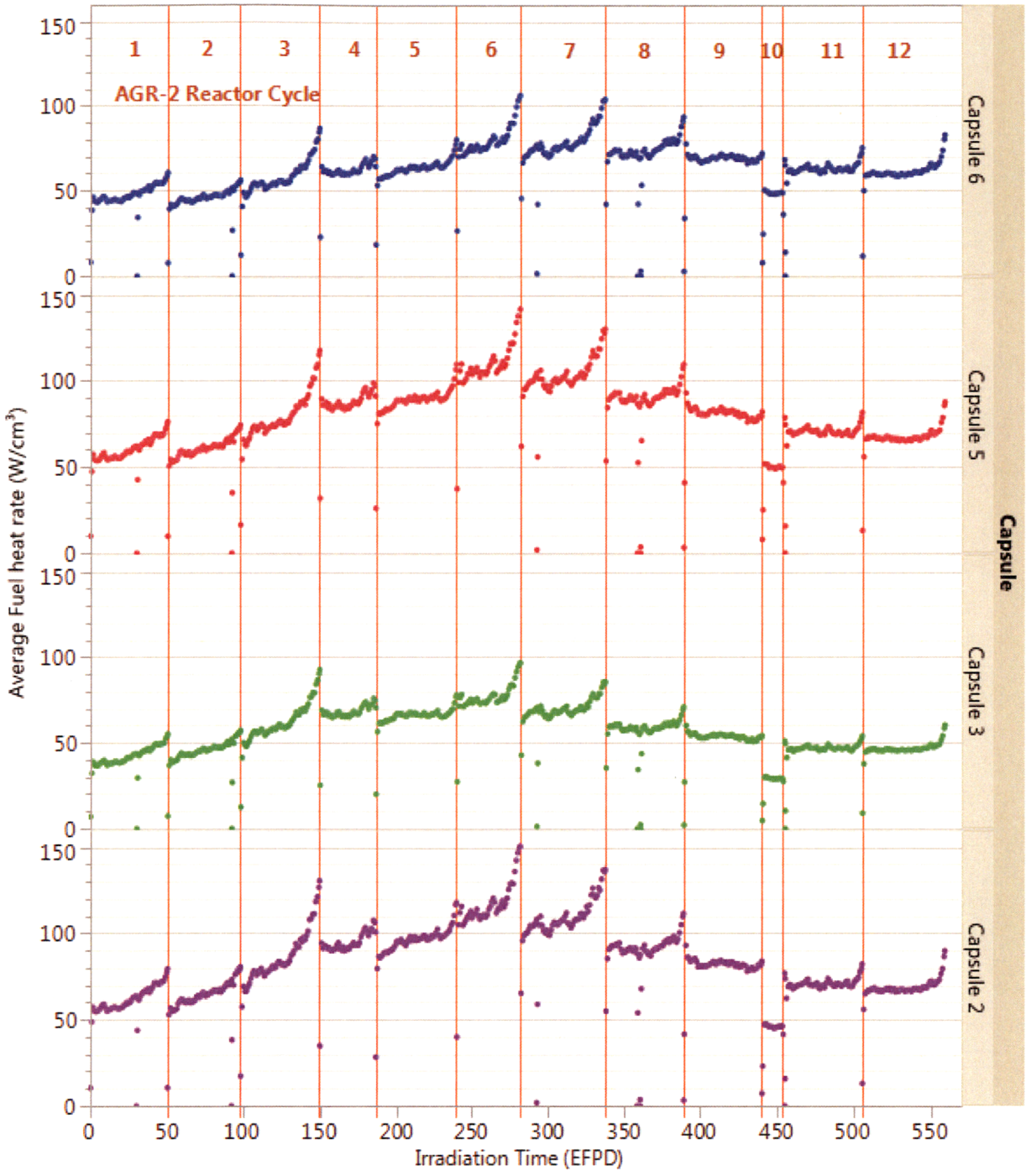

Figure 6-7
AGR-2 capsule average power density versus irradiation time in EFPDs
Courtesy of Idaho National Laboratory and used with permission of Battelle Energy Alliance, LLC

In many of the individual irradiation cycles, an increase in power density can be observed towards the end. This is because late in the cycle, outer shim cylinders (also called control drums), as shown in Figure 6-1, were often rotated such that the hafnium absorbers are oriented further away from the core to compensate for driver fuel burnup over the cycle. This operation also tends to increase the thermal flux substantially in the region of the B-10 and B-12 positions. This increase at the end of the cycle was not observed during Cycle 153B (the tenth AGR-2 power cycle) because the test train was located in the I-24 position of the ATR where the effect of the rotation of the outer shims is opposite.

These power densities are converted to maximum, minimum, and average power per particle in Figure 6-8. The power per particle ranged from 20 to 110 mW/particle in the AGR-1 irradiation. For AGR-2, which had UCO fuel particles with larger fissile kernels compared to AGR-1, the power per particle was somewhat higher and ranged from 20 to 160 mW/particle. The power per particle was even higher in the AGR-2 UO_2 capsule although the fissile inventory was less in the compact (the flux is higher in this axial position in the core relative to the U.S. AGR-2 UCO capsules so the power was greater).

Calculated burnups of the AGR-1 fuel compacts (in %FIMA) as a function of EFPDs are shown in the left pane of Figure 6-9, with vertical lines delineating the irradiation cycles. Capsule average burnup is shown for each capsule, along with the values for the peak and minimum compact in each capsule. The capsules at the top and bottom of the reactor (that is, Capsules 6 and 1, respectively) have the lowest burnup, with higher values found in the center capsules.

Capsule-average burnups ranged from 13.4% FIMA in Capsule 6 to 18.6% FIMA in Capsule 3. The right pane of Figure 6-9 shows fast neutron fluence (E >0.18 MeV) versus time in EFPDs, with vertical lines delineating the irradiation cycles. As would be expected, the trends of fast fluence follow quite closely those of burnup. The capsule with the lowest average fluence at the end of the irradiation was Capsule 6 with a value of 2.65×10^{25} n/m^2 (E >0.18 MeV), and the capsule with the highest was Capsule 3 at 4.07×10^{25} n/m^2 (E >0.18 MeV).

For AGR-2, the left pane of Figure 6-10 shows capsule-average burnups ranged from 9.3% FIMA in Capsule 6 to 12.2% FIMA in Capsule 2 for UCO. The fast neutron fluence (E >0.18 MeV) versus time in EFPDs, shown in the right pane, indicates the trends of fast fluence closely follow those of burnup.

The AGR-2 UCO capsule with the lowest average fluence at the end of the irradiation was Capsule 6 with a value of 2.39×10^{25} n/m^2, and the UCO capsule with the highest was Capsule 2 at 3.25×10^{25} n/m^2. The lower burnup of AGR-2 UCO compacts compared to AGR-1 compacts is associated with the different enrichments of the fuel particles in the two experiments (19.7% versus 14.0%). Given their low enrichment, the AGR-2 UO_2 compacts received lower peak burnup (10.7% FIMA) compared to the AGR-2 UCO fuel (13.2% FIMA).

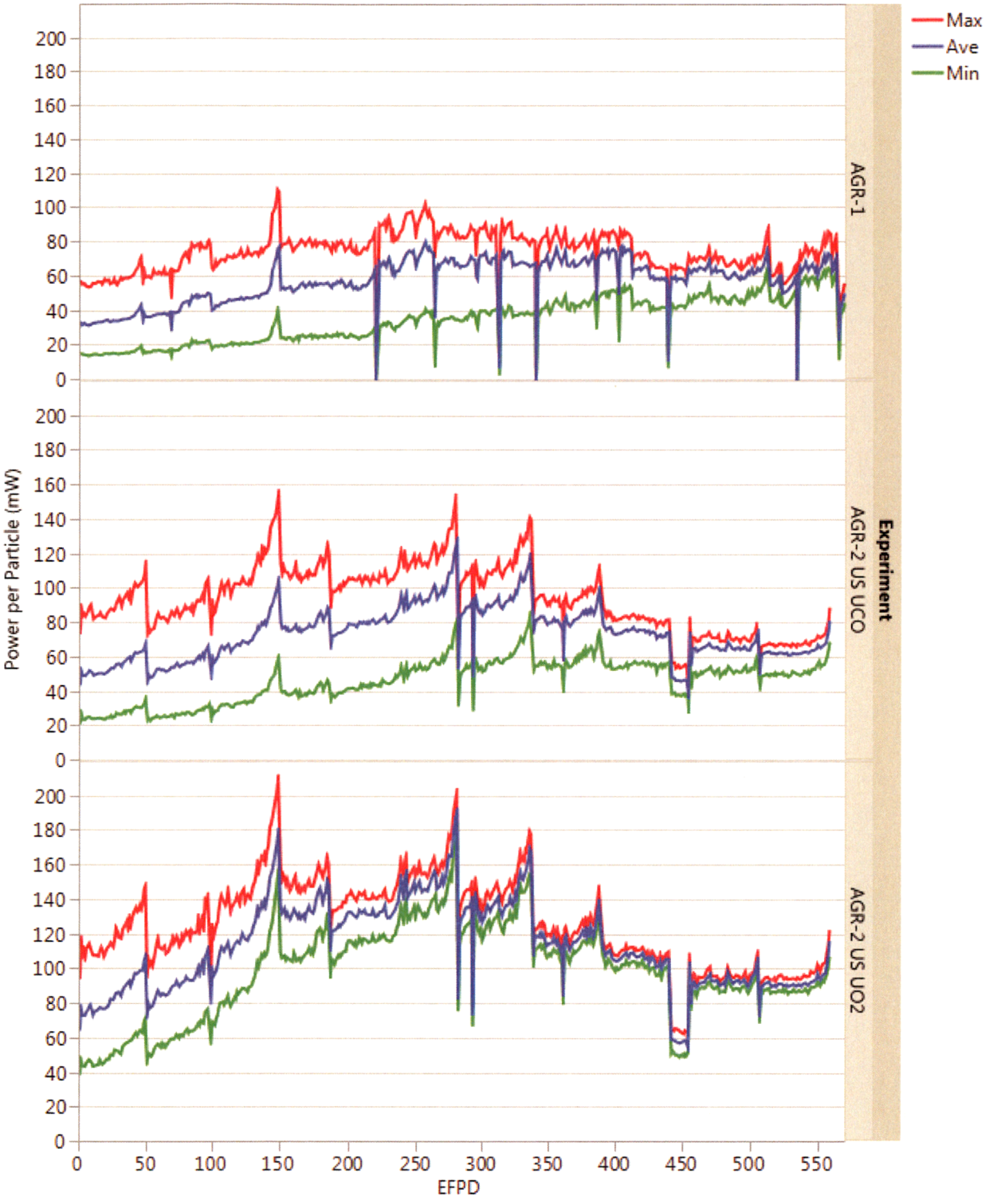

Figure 6-8
Power per particle for AGR-1 and AGR-2 irradiations
Courtesy of Idaho National Laboratory and used with permission of Battelle Energy Alliance, LLC

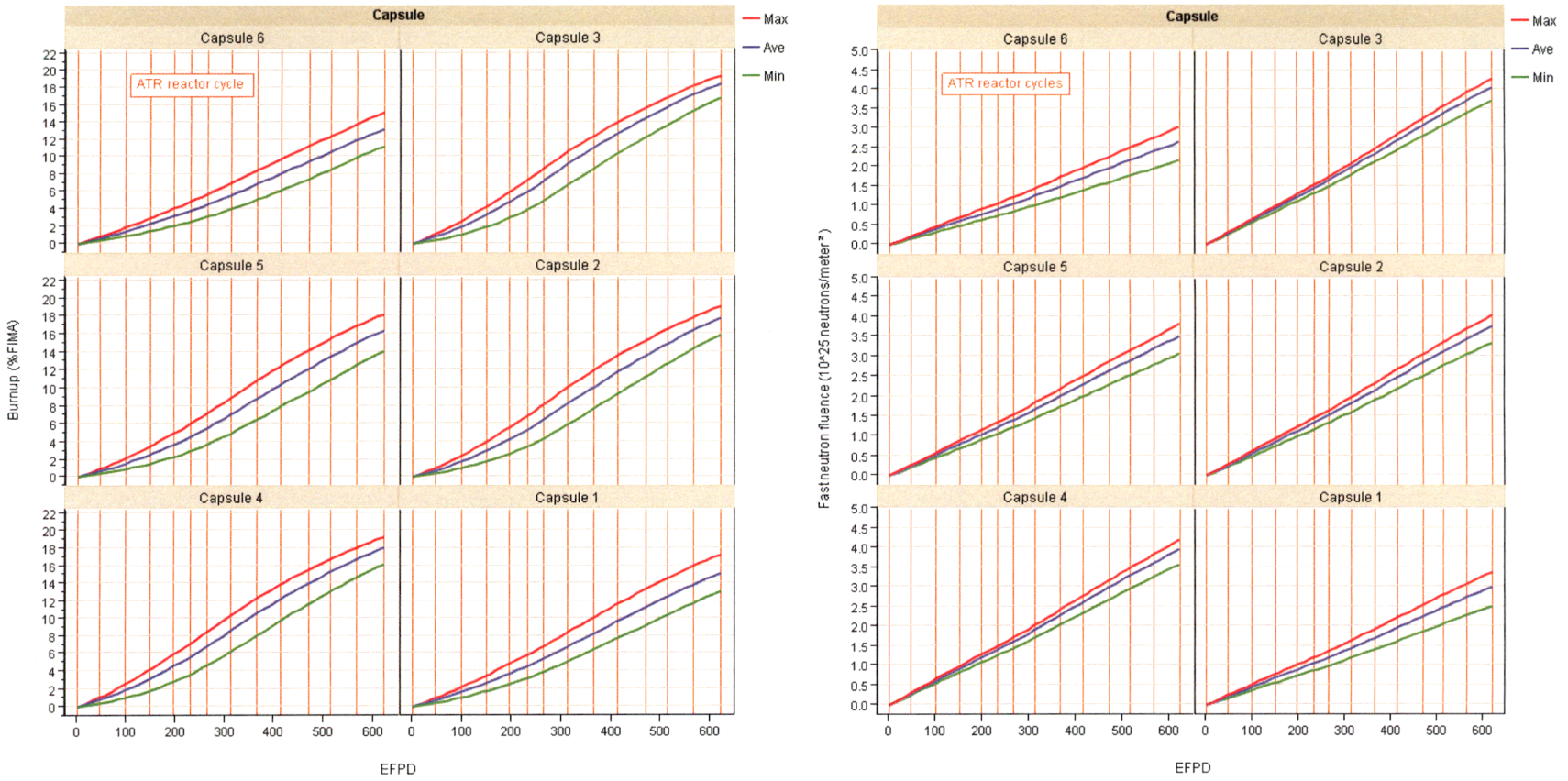

Figure 6-9
AGR-1 burnup (%FIMA) and fast neutron fluence (E >0.18 MeV) versus EFPD by capsule
Courtesy of Idaho National Laboratory and used with permission of Battelle Energy Alliance, LLC

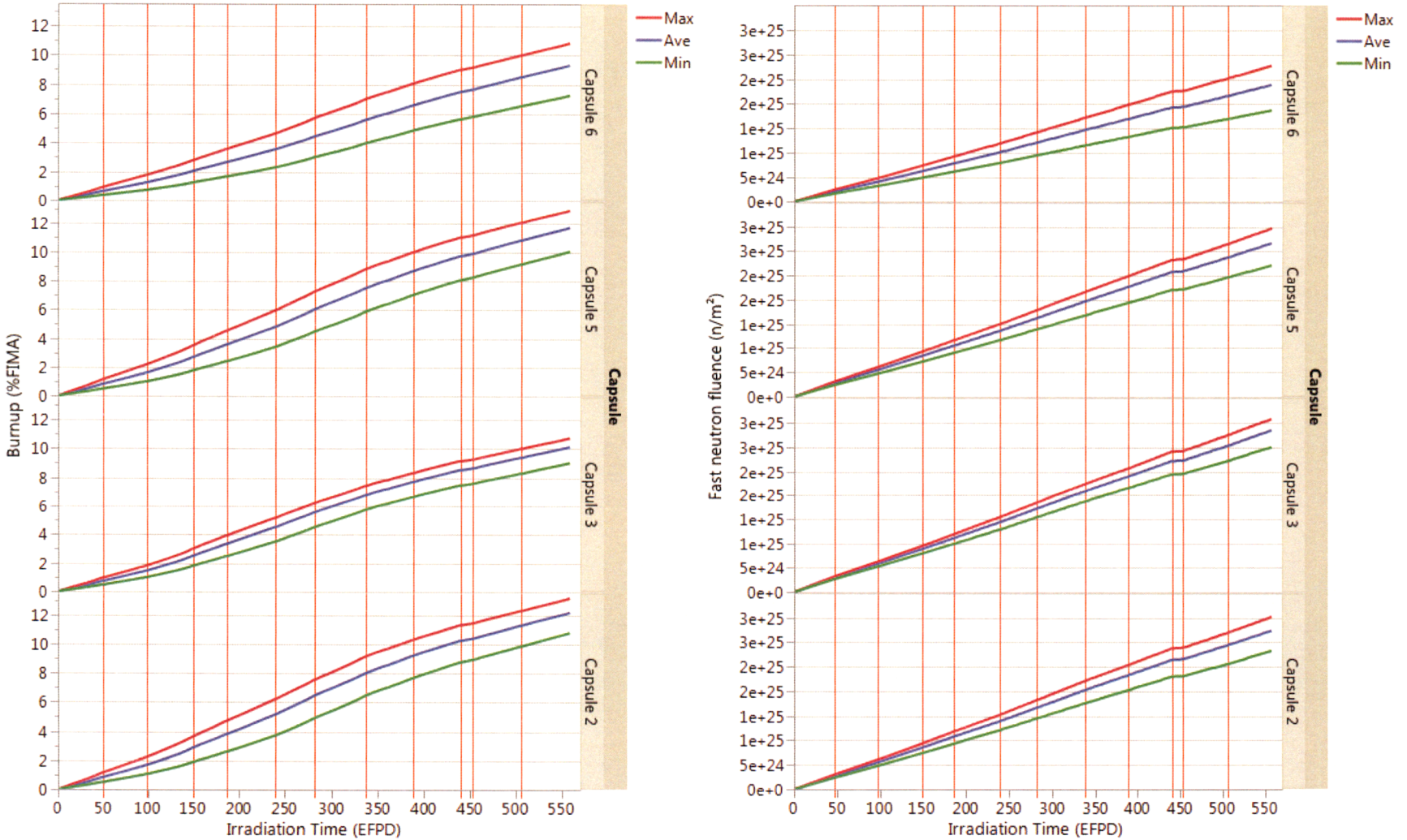

Figure 6-10
AGR-2 burnup (%FIMA) and fast neutron fluence (E >0.18 MeV) versus EFPD by capsule
Courtesy of Idaho National Laboratory and used with permission of Battelle Energy Alliance, LLC

Figure 6-11 shows the correlation between burnup and fast fluence for the 72 AGR-1 compacts and the 48 AGR-2 compacts. The minimum, average, and maximum burnups of the AGR-1 and AGR-2 compacts by capsule are tabulated in Table 6-1. Collectively, the AGR-1 and AGR-2 irradiations provided compacts with a broad range of irradiation conditions with which to elucidate the performance of TRISO-coated UCO particles.

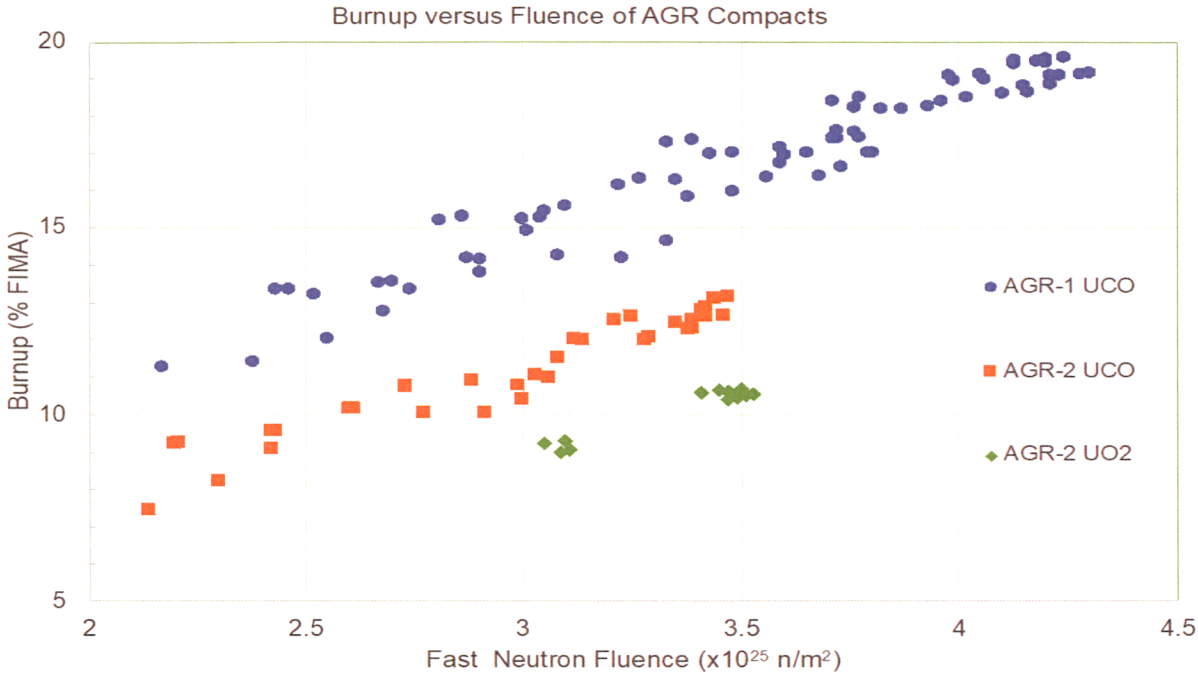

Figure 6-11
Fast neutron fluence (E >0.18 MeV) vs. burnup (%FIMA) for AGR-1 and AGR-2 compacts
Courtesy of Idaho National Laboratory and used with permission of Battelle Energy Alliance, LLC

Both the AGR-1 and AGR-2 experiments contained fluence wires embedded in the graphite sample holders in each capsule. Analysis of the fluence wires yielded the thermal and fast fluence that accumulated during the irradiation. The wires were gamma counted to determine the inventory of the relevant activation products. Following gamma counting, the packages containing the niobium wires were opened, and the wires were removed and dissolved in acid. Aliquots of the solution were placed on filter paper for x-ray counting using low-energy photon spectrometers. The inventory of five different isotopes were ultimately determined for the wires (that is, ^{54}Mn, ^{59}Fe, ^{60}Co, ^{93m}Nb, ^{94}Nb), and these were used to calculate neutron fluences in the capsules in the thermal, epithermal, and fast energy ranges.

Table 6-1
AGR-1 and AGR-2 minimum, average, and peak compact burnup and fast fluence at the end of irradiation

Capsule	Compact Burnup (% FIMA)			Compact Fast Neutron Fluence (10^{25} n/m^2 E >0.18 MeV)		
	Minimum Compact	Capsule Average	Peak Compact	Minimum Compact	Capsule Average	Peak Compact
AGR-1 UCO						
1	13.2	15.3	17.4	2.52	3.02	3.39
2	16.0	17.8	19.1	3.35	3.77	4.05
3	17.0	18.6	19.6	3.72	4.07	4.30
4	16.4	18.2	19.4	3.59	3.98	4.21
5	14.2	16.5	18.2	3.08	3.52	3.82
6	11.3	13.4	15.3	2.17	2.65	3.04
AGR-2 UCO						
2	10.8	12.2	13.2	2.88	3.25	3.47
5	10.1	11.7	12.9	2.77	3.18	3.42
6	7.3	9.3	10.8	1.94	2.39	2.73
AGR-2 UO_2						
3	9.0	10.1	10.7	3.05	3.35	3.53

For the AGR-1 experiment, the results for fast neutron fluence (E >0.18 MeV) based on fluence wire measurements have been compared with the predicted values from the as-run AGR-1 physics calculations for each capsule (with the exception of Capsule 1, for which no fluence wires were recovered). The comparison is shown in Table 6-2. The results demonstrated excellent agreement, as the difference between values from the two methods was within <7% for all five capsules compared.

Table 6-2
Comparison of AGR-1 capsule fast neutron fluence (E >0.18 MeV) determined from measurement of fluence wires and from physics calculations [72]

Capsule	Fast fluence (10^{25} n m^{-2})		Difference
	Measured	Calculated	
6	2.33 ± 7%	2.42	+3.7%
5	3.06 ± 7%	3.05	−0.3%
4	3.25 ± 7%	3.43	+5.2%
3	3.33 ± 7%	3.39	+1.8%
2	3.19 ± 7%	2.99	−6.7%
1	–	2.29	–

Burnup of compacts from both experiments was determined experimentally using nondestructive gamma spectrometry and agreement with calculated values across all compacts in the experiments is good [73,74]. Burnup was also determined in selected fuel compacts from the AGR-1 experiment through dissolution of fuel kernels and mass spectrometry measurements. Similar measurements on AGR-2 fuel are in progress. Table 6-3 shows the comparison between measured and calculated burnup values for four AGR-1 compacts [72,75]. Note that two different approaches were used to derive burnup values using gamma spectrometry data [75].

Table 6-3
Comparison of measured and calculated burnup values for AGR-1 fuel compacts

Compact	Mass Spectrometry	Gamma Spectrometry Direct	Gamma Spectrometry Ratio	Calculated
6-3-2	10.7 (±0.5) %	10.7 (±0.5) %	11.0 (±0.3) %	11.31%
3-2-1	19.3 (±1.0) %	18.2 (±0.9) %	18.6 (±0.6) %	18.98%
5-3-1	16.3 (±0.8) %	16.9 (±0.8) %	15.9 (±0.5) %	16.88%
1-3-1	16.3 (±0.8) %	16.0 (±0.8) %	15.6 (±0.5) %	15.98%

6.3 Thermal Analysis

The temperature at which the fuel compacts were irradiated is an essential component of assessing the performance of the fuel. 3-D finite element thermal calculations were performed on a daily basis using Abaqus FEA [76,77]. These calculations were performed using compact heat generation rates provided by the as-run neutronics analysis described earlier and with additional operational input for sweep gas composition versus time. Figure 6-12 shows a cross section of the AGR-2 finite element mesh formed from eight-node hexahedral bricks. The model contains approximately 350,000 nodes per capsule for both AGR-1 and AGR-2.

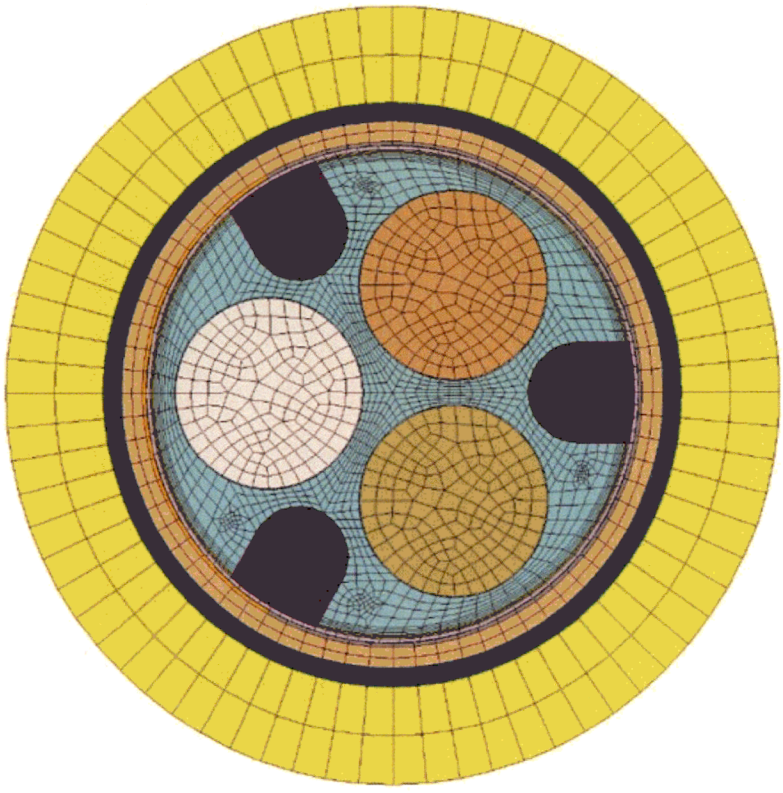

Figure 6-12
Two-dimensional cross-section of Abaqus FEA model for AGR-2 irradiation
Courtesy of Idaho National Laboratory and used with permission of Battelle Energy Alliance, LLC

Figure 6-13 shows a sample temperature profile calculated by Abaqus FEA after ~250 EFPDs in AGR-1 Capsule 4 (top) and after 290 EPPDs in AGR-2 Capsule 3 (bottom). Higher temperatures were in the center of the fuel stacks, with lower temperatures on the edges that were closer to the periphery of the capsule. The lowest temperatures were found on the compacts in Stack 2 on the left in the top pane of Figure 6-13 (AGR-1) since it was the compact furthest away from the ATR core. Because AGR-2 was a mirror image of AGR-1, the compacts in Stack 3 had the lowest temperatures as this stack was facing away from the core.

Figures 6-14 and 6-15 show the daily calculated fuel temperatures (capsule volume average, capsule maximum, and capsule minimum) for each of the six AGR-1 capsules versus time in EFPDs, Figures 6-16 and 6-17 show the time-average values of these temperatures plotted as a function of time for the six AGR-1 capsules. Similar plots are shown in Figures 6-18 and 6-19 for the U.S. AGR-2 capsules.

The end-of-irradiation time-average temperatures are summarized for each capsule in Table 6-4. In this table, the values listed are the lowest of the time-average minimum temperatures for the 12 compacts, the highest of the time-average maximum temperatures, and the average of the time-average, volume-average temperatures for the compacts. Thus, the table indicates, for example, the highest compact time-average maximum temperature in AGR-2 Capsule 2 was 1360°C and the lowest compact time-average minimum temperature was 1034°C.

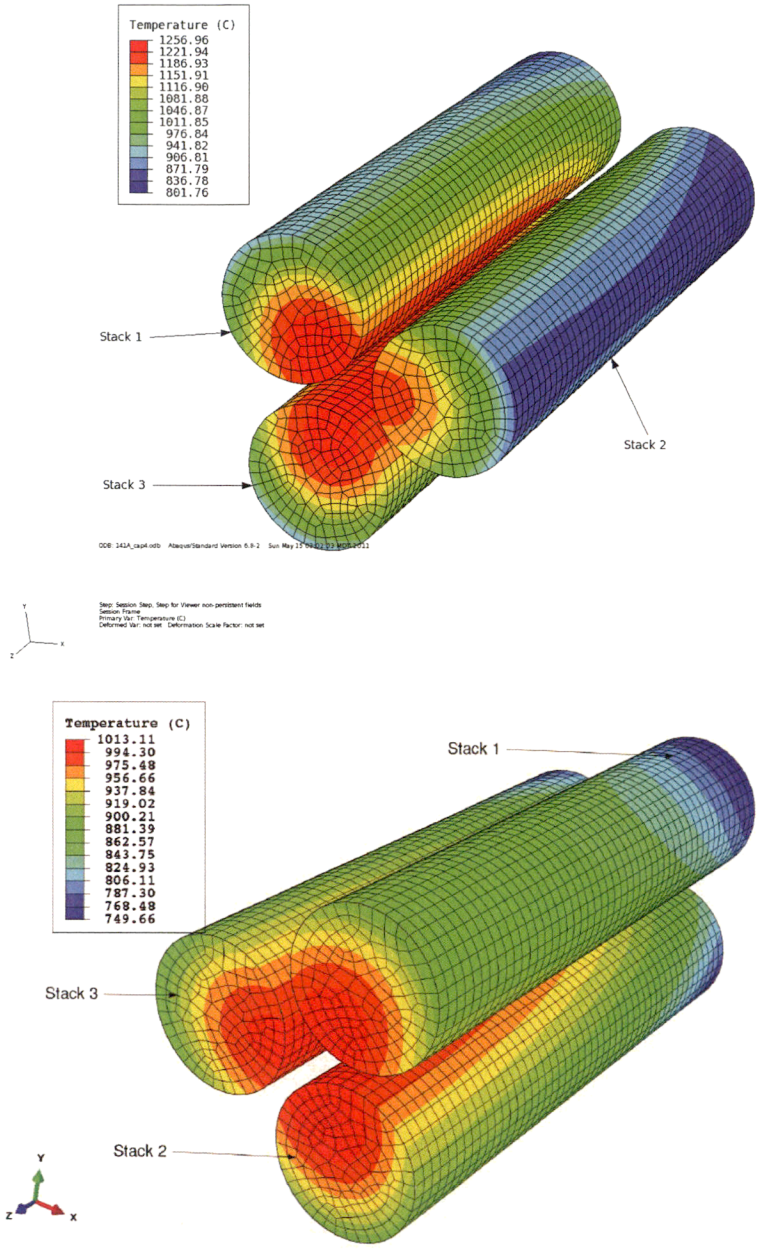

Figure 6-13
Sample temperature profile in AGR-1 Capsule 4 after ~250 EFPDs (top) and AGR-2 Capsule 3 after 290 EFPDs (bottom)
Courtesy of Idaho National Laboratory and used with permission of Battelle Energy Alliance, LLC

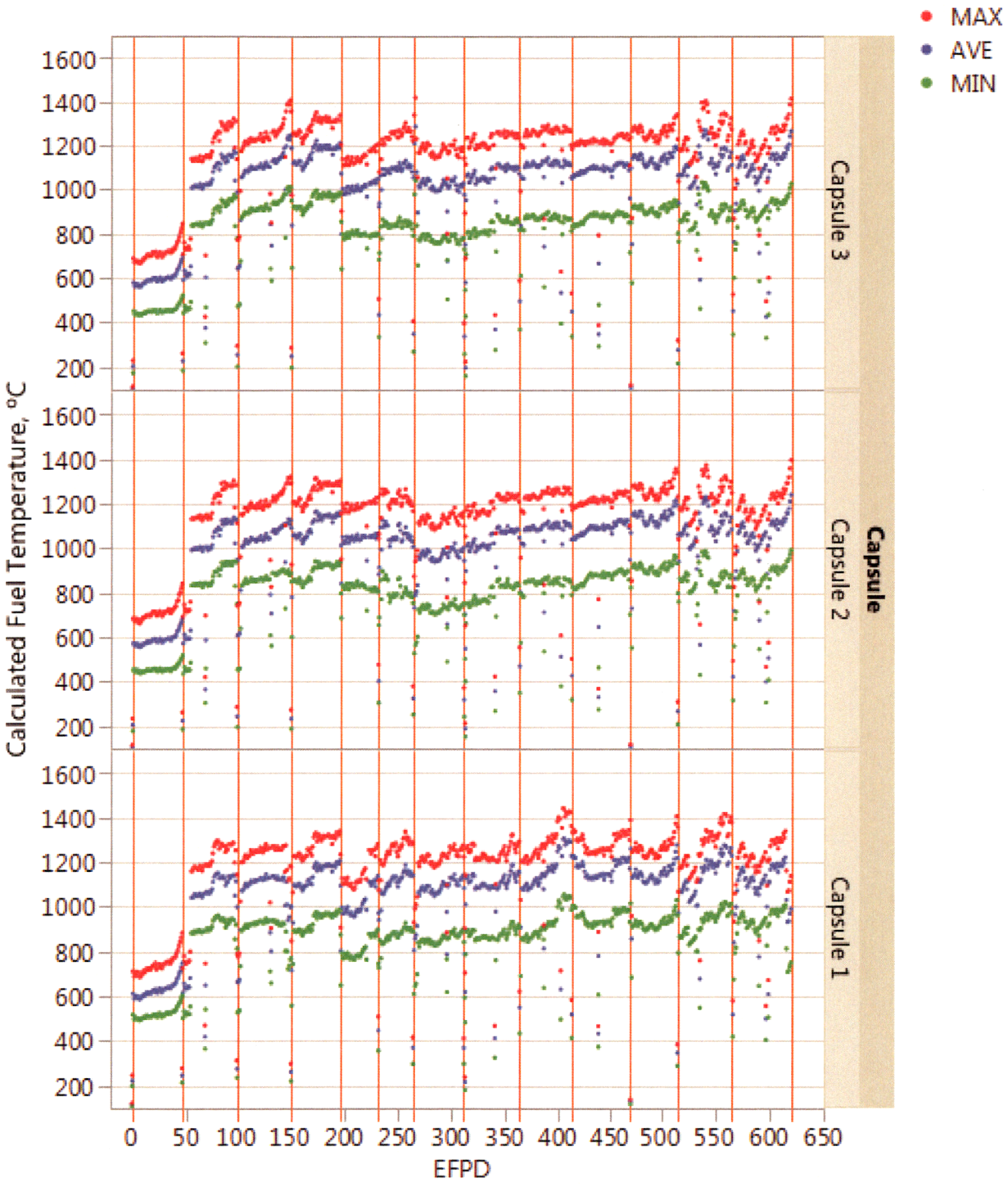

Figure 6-14
AGR-1 calculated daily minimum, maximum and volume average temperatures for capsules 1-3
Courtesy of Idaho National Laboratory and used with permission of Battelle Energy Alliance, LLC

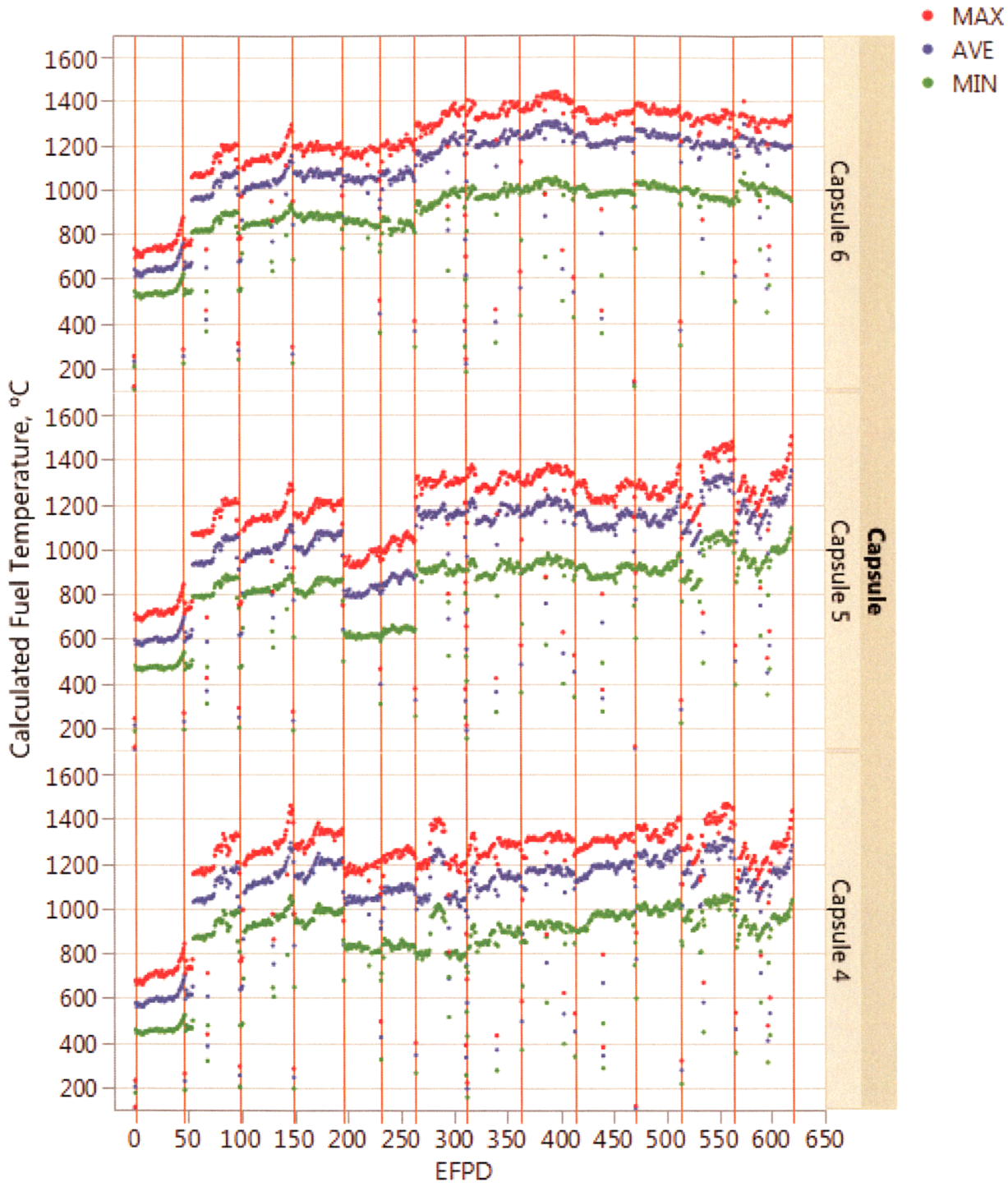

Figure 6-15
AGR-1 calculated daily minimum, maximum, and volume average temperatures for capsules 4-6
Courtesy of Idaho National Laboratory and used with permission of Battelle Energy Alliance, LLC

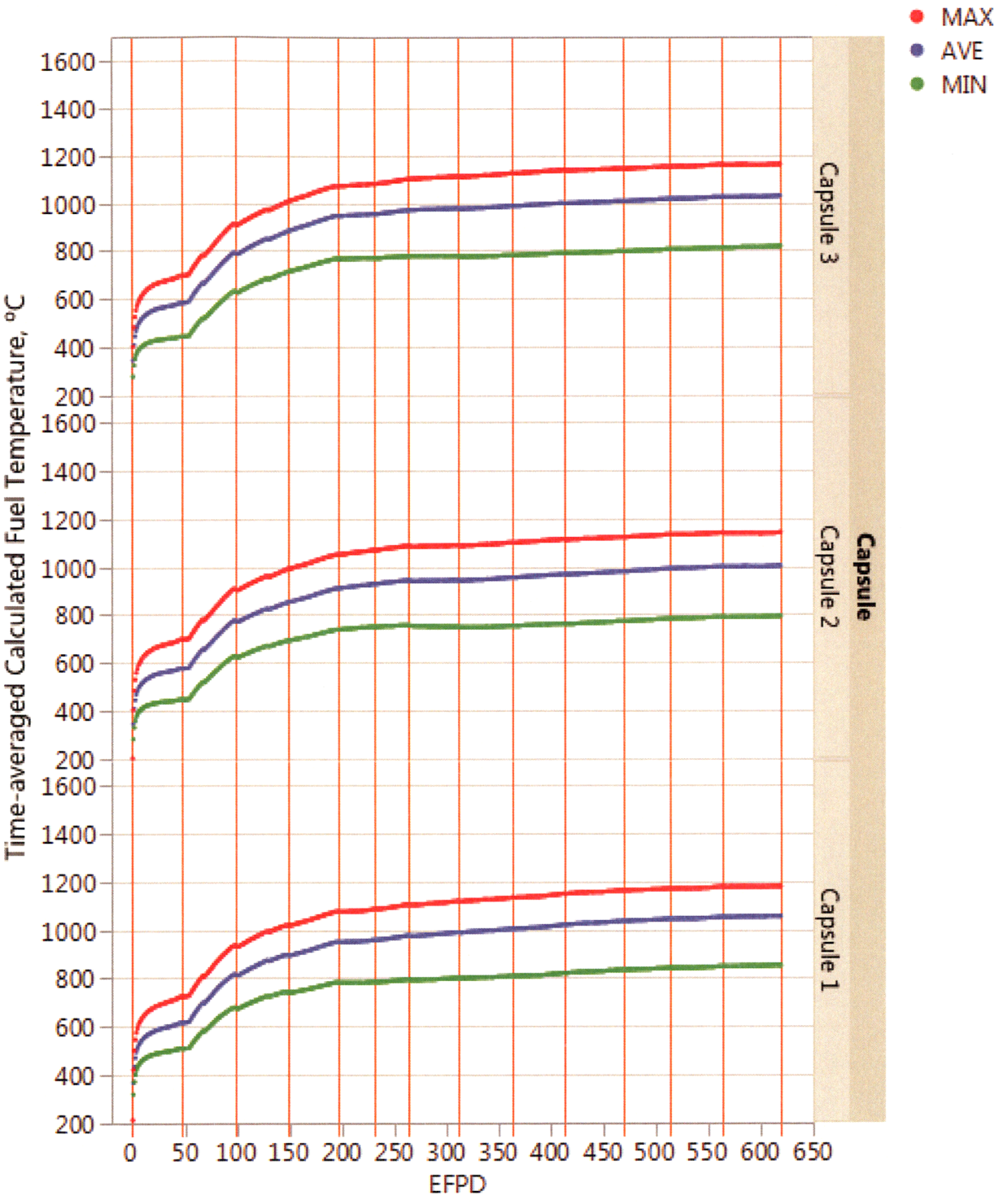

Figure 6-16
AGR-1 calculated time-average minimum, time-average maximum and time-average volume-average temperatures for capsules 1-3
Courtesy of Idaho National Laboratory and used with permission of Battelle Energy Alliance, LLC

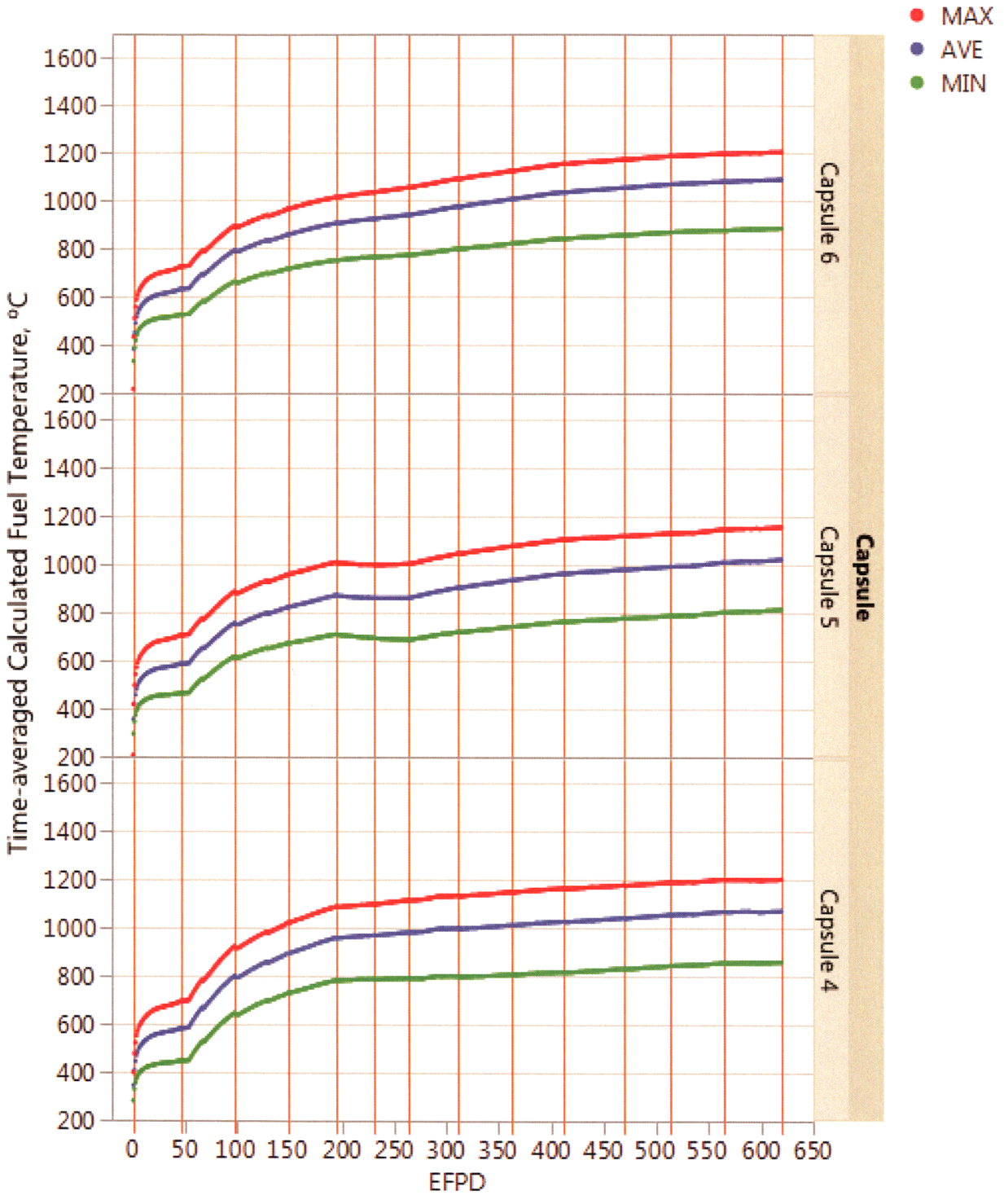

Figure 6-17
AGR-1 calculated time-average minimum, time-average maximum and time-average volume-average temperatures for capsules 4-6
Courtesy of Idaho National Laboratory and used with permission of Battelle Energy Alliance, LLC

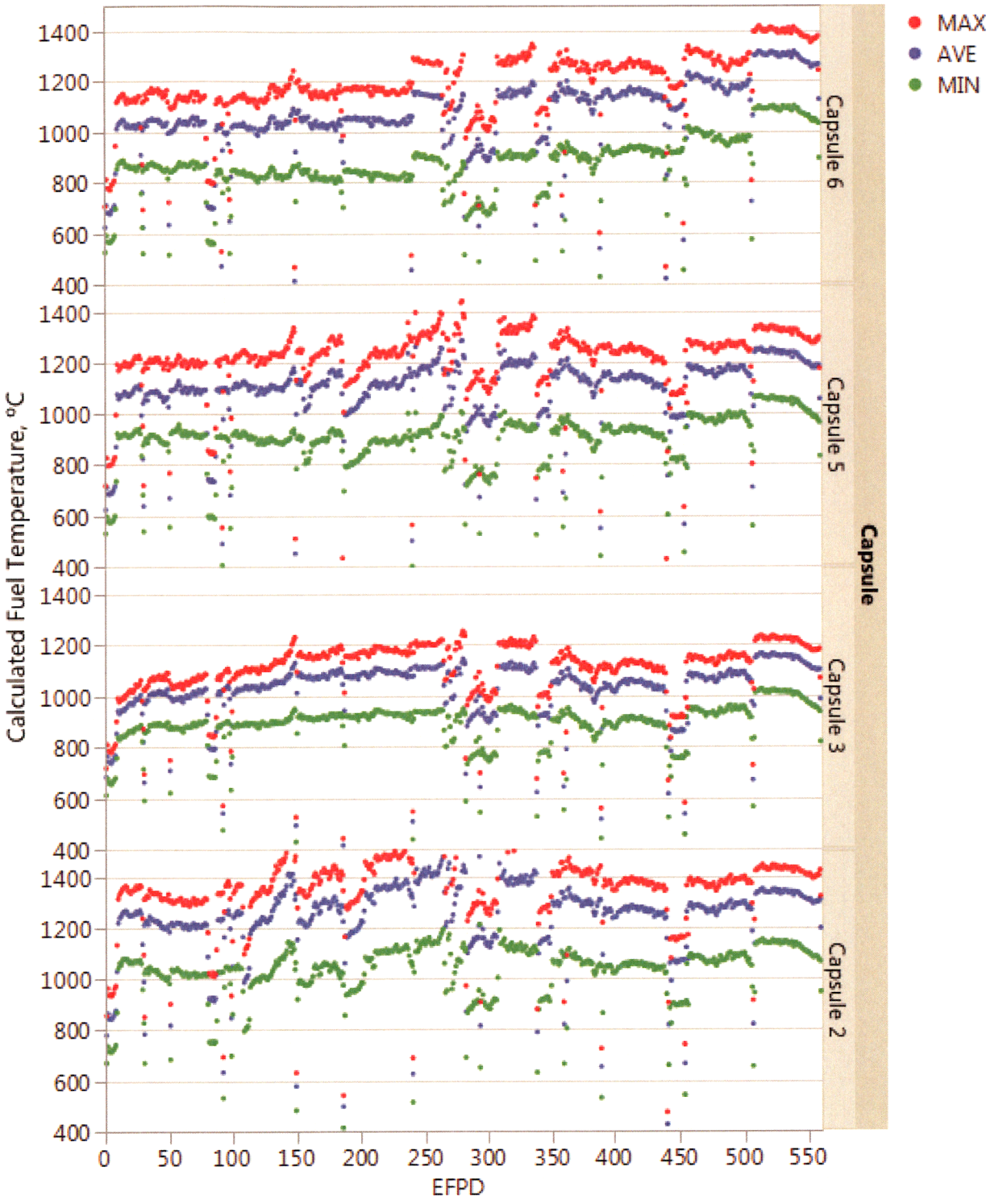

Figure 6-18
AGR-2 calculated daily minimum, maximum, and volume average temperatures
Courtesy of Idaho National Laboratory and used with permission of Battelle Energy Alliance, LLC

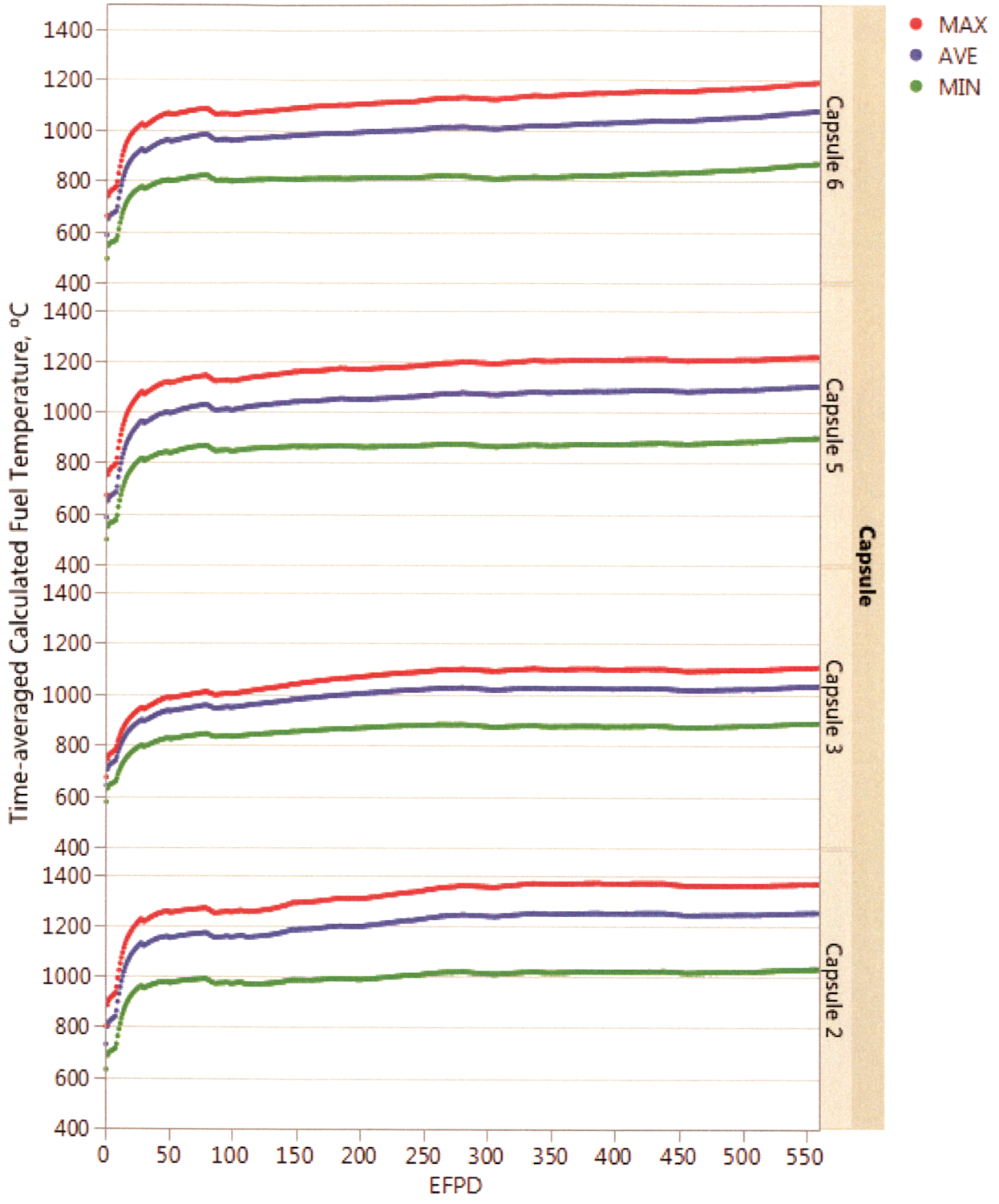

Figure 6-19
AGR-2 calculated time-average minimum, time-average maximum, and time-average volume-average temperatures
Courtesy of Idaho National Laboratory and used with permission of Battelle Energy Alliance, LLC

Table 6-4
End-of-irradiation time-average temperatures for AGR-1 and AGR-2 capsules

Capsule Number	Time-Average Minimum Temperature (°C)	Time-Averaged Volume-Average Temperature (°C)	Time-Average Maximum Temperature (°C)
AGR-1 UCO			
1	854	1054	1167
2	800	1002	1124
3	828	1028	1147
4	866	1070	1187
5	818	1023	1144
6	885	1087	1197
AGR-2 UCO			
2	1034	1252	1360
5	901	1101	1210
6	868	1074	1183
AGR-2 UO_2			
3	889	1032	1105

6.4 Thermocouple Measurement and Performance

Temperature measurements for both AGR-1 and AGR-2 were performed by TCs terminating within the graphite sample holders of each capsule. These measurements supported temperature control of the experiment where designated control TCs provided feedback to the automated sweep gas control system that adjusted gas blends to maintain reference temperatures. TC measurements are also used to support thermal analyses of the test train, which are used to calculate fuel temperatures. When a control TC failed during the irradiation, a previously selected back-up TC within the same capsule was used as the control TC and the reference control temperature reset based on thermal analysis calculations. When all TCs failed within a capsule, results from physics and thermal analyses, and operating history of adjacent capsules were used to manually set the gas blends of the affected capsule.

The AGR-1 test train was designed with 19 TCs; three TCs failed during fabrication and seven more failed during operation. The two failure mechanisms for the TCs were the formation of virtual junctions and open circuit failures where the signal ceases altogether. Virtual junctions are detected by perturbing the temperature in a single capsule using gas flow, then observing the TC readings from capsules below this one to see if they respond. If a capsule TC responds to temperature changes in a capsule above it, it is likely a virtual junction has formed, and the TC can be considered failed. TC-2 in Capsule 5 was damaged during fabrication of the test train and was never operational. By the end of irradiation, all TCs in Capsules 1, 2, and 3, plus TC-3 in Capsule 4, had been declared failed.

The AGR-2 TCs did not perform as well as in AGR-1. Fewer TCs were used in AGR-2 than in AGR-1, but their diameters were larger to accommodate larger thermo-elements, which were expected to provide better survivability. The sheath material was changed from the Inconel 600 used in AGR-1 to niobium. It is hypothesized the sheaths became brittle during irradiation and started fracturing in the later stages of irradiation due to both thermal expansion and contraction upon heat-up and cool-down, as well as from handling of the test train when it was moved for high-power cycles in ATR, causing the TCs to fail. Of the 11 TCs in Capsules 2, 3, 5, and 6, one failed during fabrication and the other 10 TCs failed during operation between the second and final AGR-2 irradiation cycles. All TC failures were attributed to open circuit failure, which is typically caused by breakage of a thermo-element wire or the junction itself. However, temperature control of all capsules was maintained using thermal analysis calculations that were benchmarked against the TC measurements before the TCs failed.

TC drift was assessed by analysis, which used as-run sweep gas mixes and heat generation rates from physics analyses, where thermal model results for the specific TC location were compared to TC readings. Figure 6-20 shows the differences between the measured and calculated TC temperatures in the AGR-1 irradiation while the TCs were considered operational. Data are not shown for TCs after they were declared failed. A downward drift of measured TC temperatures relative to calculated TC temperatures over irradiation time can be observed in TC-2 (red dots in Figure 6-20) in Capsules 2, 3, and 4. Readings from other TCs are consistent with their simulation results. The differences between what was measured and what was calculated was generally within ±100°C, although this threshold was exceeded in some instances, particularly in the second half of the irradiation.

Similar results are shown in Figure 6-21 for AGR-2. TC-3 in Capsule 6, and to a lesser extent TC-2 and TC-5 in Capsule 6, show evidence of drift. Except for TC-3 in Capsule 6, the agreement between the measured and calculated TC temperatures for the UCO capsules were within ±100°C. For Capsule 3 (UO_2 fuel) the agreement is much better, within ±20-50°C.

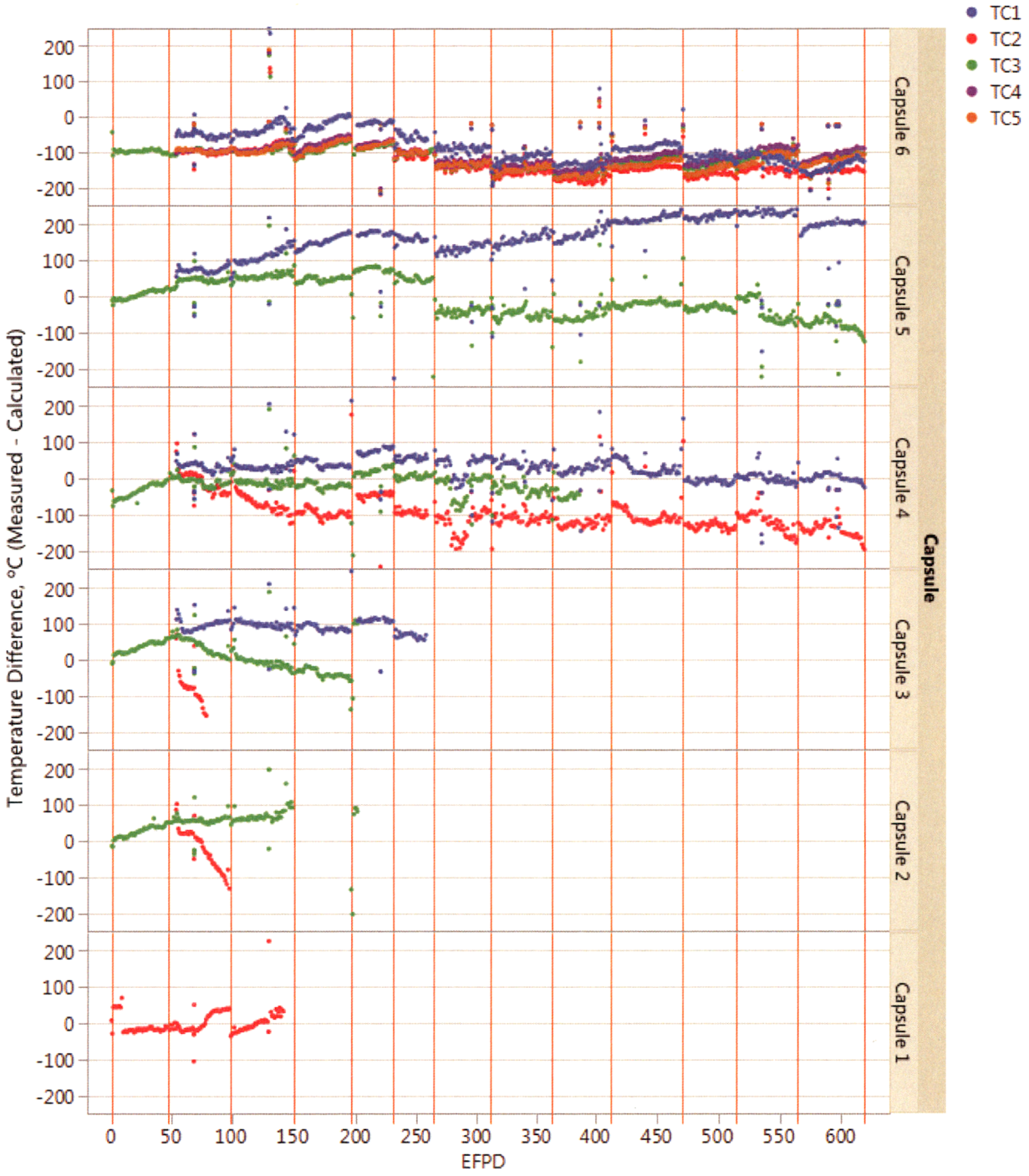

Figure 6-20
Difference between measured and calculated TC temperatures for AGR-1 versus EFPDs
Courtesy of Idaho National Laboratory and used with permission of Battelle Energy Alliance, LLC

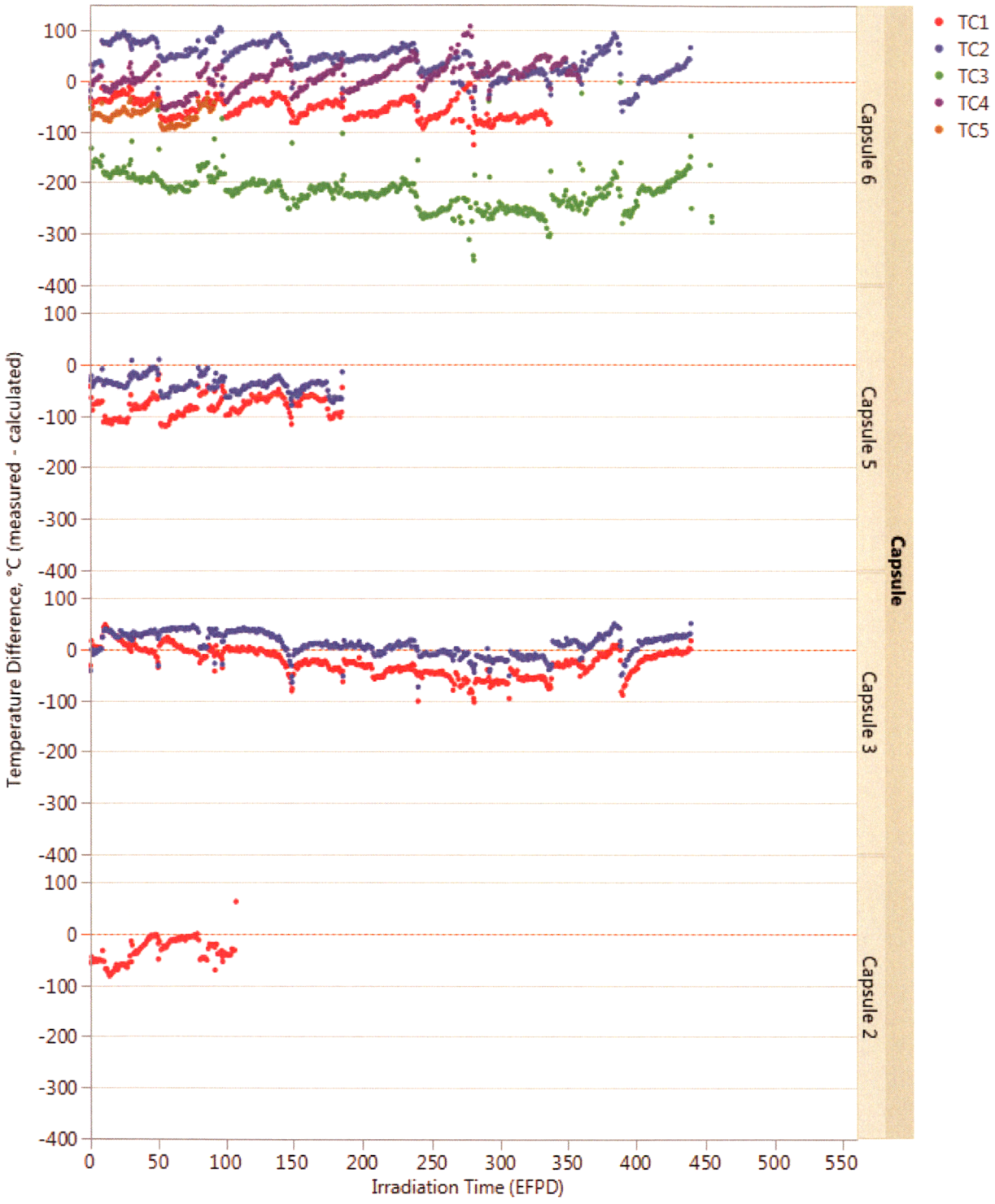

Figure 6-21
Difference between measured and calculated TC temperatures for AGR-2 versus EFPDs
Courtesy of Idaho National Laboratory and used with permission of Battelle Energy Alliance, LLC

6.5 Uncertainty Quantification of Calculated Temperatures

An uncertainty analysis has been performed for the temperature estimates in AGR-1 using a formal uncertainty propagation protocol that considers both the traditional uncertainties of each key variable used in the calculation, but also includes the first order cross-correlation effects of the key variables in the uncertainty estimates [78, 79]. The uncertainties in predicted temperatures using this approach change over the course of the irradiation since uncertainties in key inputs like gas gap size increased with time due to carbonaceous matrix shrinkage (primarily an effect of accumulated fast fluence) and fuel heat rate changes due to fissile burnup and changes in ATR operation. The uncertainties also vary by capsule and experiment given the different gas gap sizes used in each capsule. The results identify those input parameters having the greatest impact on the overall uncertainty, which has been helpful in designing the follow-on capsules.

To quantify the uncertainty of AGR-1 calculated temperatures, the uncertainty assessment identified and analyzed Abaqus FEA model parameters of potential importance to the AGR-1 predicted fuel temperatures. Specifically, the key variables include: (1) the width of the control gas gap; (2) the neon gas fraction; (3) the fuel heat rate; (4) the graphite holder thermal conductivity; and (5) the fuel compact thermal conductivity. Expert judgments were used as a basis to specify the uncertainty range for a set of select parameters, including those with high sensitivity and those with large uncertainty. The overall effect of a parameter uncertainty on the model prediction variation is a product of input uncertainty and its sensitivity coefficient. Propagation of model parameter uncertainty was then used to quantify the overall uncertainty of AGR-1 calculated temperatures.

The overall uncertainty in the calculated temperatures for AGR-1 ranged from 2.0 to 6.5% (~40 to 60°C at 1σ and 100 to 120°C at 2σ), depending on irradiation time (thermal conditions), capsule, and the temperature parameter being predicted (for example, peak fuel temperature, volume-average fuel temperature, or TC temperature). Table 6-5 presents temperatures and their relative and absolute standard deviations for TAVA and time-average maximum fuel temperatures at the end of AGR-1 for six capsules.

Table 6-5
Temperatures (T) and uncertainty (σ_T) for time-average fuel temperatures at the end of AGR-1[a]

Capsule	Time-Average Volume-Average Fuel			Time-Average Maximum Fuel		
	T, °C	σ_T, %	σ_T, °C	T, °C	σ_T, %	σ_T, °C
Capsule 6	1088	5.014	55	1204	5.012	60
Capsule 5	1023	3.700	38	1157	4.301	50
Capsule 4	1070	3.743	40	1202	4.327	52
Capsule 3	1029	3.777	39	1162	4.330	50
Capsule 2	1003	3.830	38	1141	4.379	50
Capsule 1	1055	3.165	33	1178	3.776	45

[a]Temperatures differ from those reported in Table 6-4 and in the AGR-1 Irradiation Test Final As-Run Report [59] due to the method used to convert daily temperature data to capsule-average and capsule-maximum values [79].

In some cases, the uncertainty is dominated by uncertainty in fuel heat rate (for example, Capsule 6). For peripheral TCs, the uncertainty is driven by the increasing uncertainty of the control gas gap distance, especially for the middle capsules at the end of irradiation. The increase of gap uncertainty has more effect on the temperature uncertainty of peripheral TCs than on the uncertainty of the center TC. The fuel temperature uncertainty is dominated by uncertainties in fuel and graphite thermal conductivity. The center TC uncertainty is dominated by uncertainties in graphite thermal conductivity.

The daily capsule volume-average and capsule peak temperatures, along with one standard deviation (indicated by the shaded regions) in AGR-1 Capsule 4 are presented in Figure 6-22 (instantaneous) and Figure 6-23 (time-average) as illustrations.

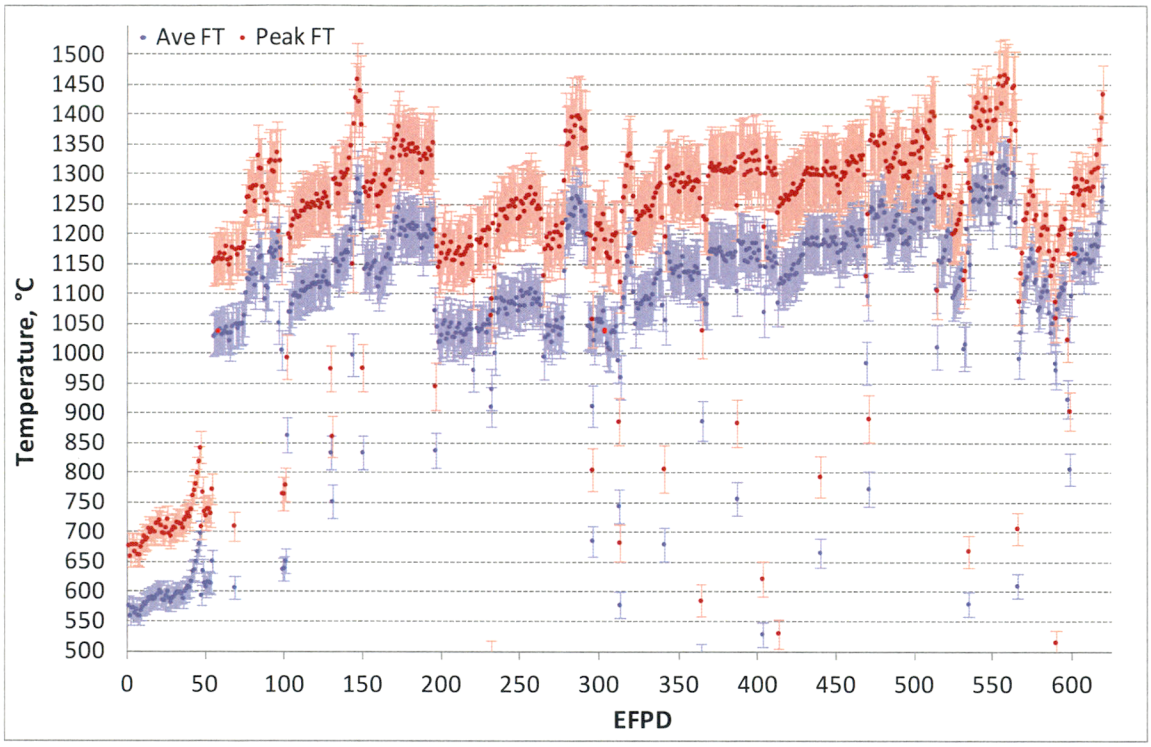

Figure 6-22
Instantaneous peak and average fuel temperature (FT) and associated uncertainty for AGR-1 Capsule 4
Courtesy of Idaho National Laboratory and used with permission of Battelle Energy Alliance, LLC

A similar analysis was performed for the AGR-2 capsules [80]. Uncertainties in the fuel heat rate and gas gap dominate the uncertainties in the time-average volume-average temperatures and in TC temperatures. The fuel and graphite thermal conductivities have minor impacts on the TC uncertainty. Uncertainties at one sigma range from 30°C to 40°C for the TAVA temperatures and 35°C to 45°C for the time-average maximum temperatures, similar to AGR-1.

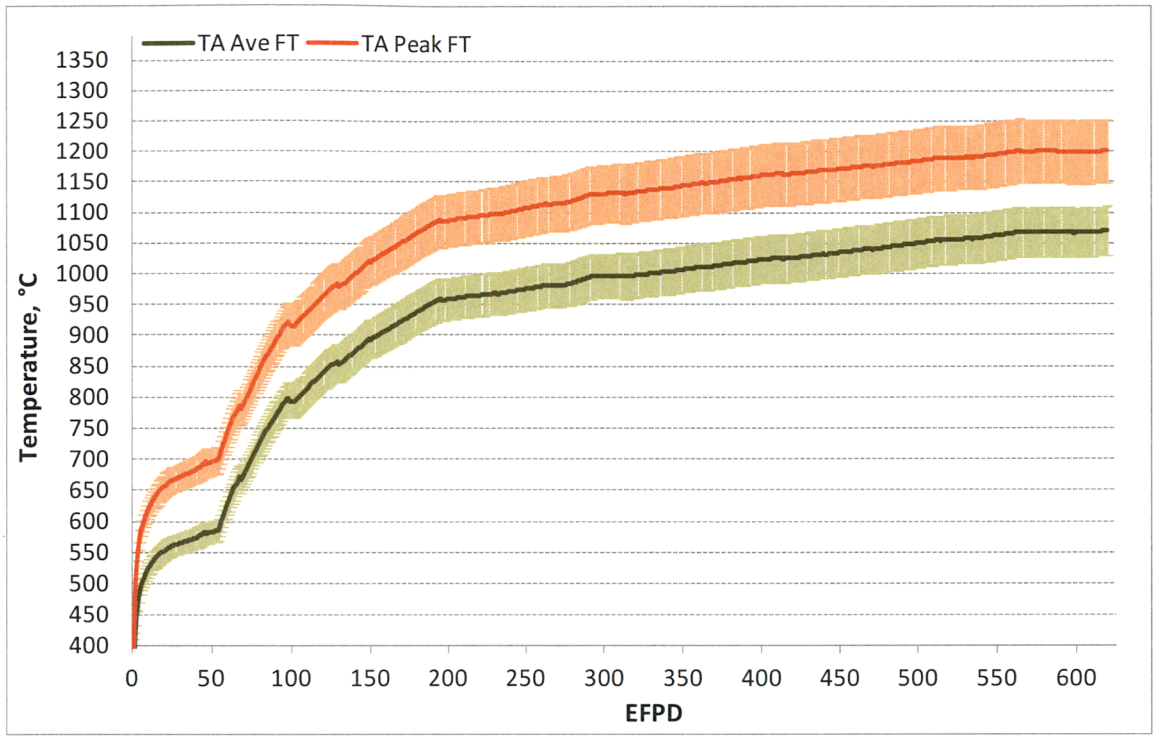

Figure 6-23
Time-average (TA) peak and time-average volume-average fuel temperatures (FT) for AGR-1 Capsule 4
Courtesy of Idaho National Laboratory and used with permission of Battelle Energy Alliance, LLC

6.6 Broader Comparisons of Key Service Conditions

The fuel particles in both AGR-1 and AGR-2 experienced a range of burnups, TAVA temperatures, and fluences during their exposure in ATR. The particles in AGR-1 and AGR-2 also experienced a broad range of temperature-burnup-fluence trajectories under irradiation, which serve as a solid foundation to demonstrate the performance of UCO TRISO-coated particles for use in HTRs. The distribution of individual fuel compact TAVA temperatures and burnup is highlighted in Figure 6-24 and the distribution of TAVA temperatures and fast fluence is highlighted in Figure 6-25. The data demonstrate the approximately 200°C distribution in temperatures for all of the fuel with the exception of AGR-2 Capsule 2, which had appreciably higher temperatures.

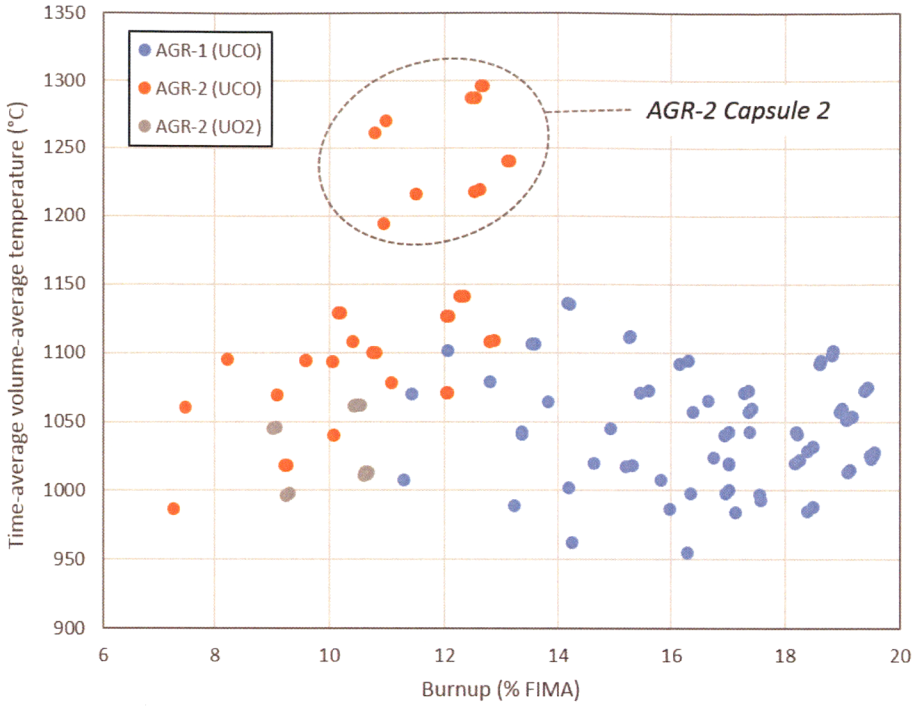

Figure 6-24
AGR-1 and AGR-2 fuel compact TAVA temperatures as a function of burnup
Courtesy of Idaho National Laboratory and used with permission of Battelle Energy Alliance, LLC

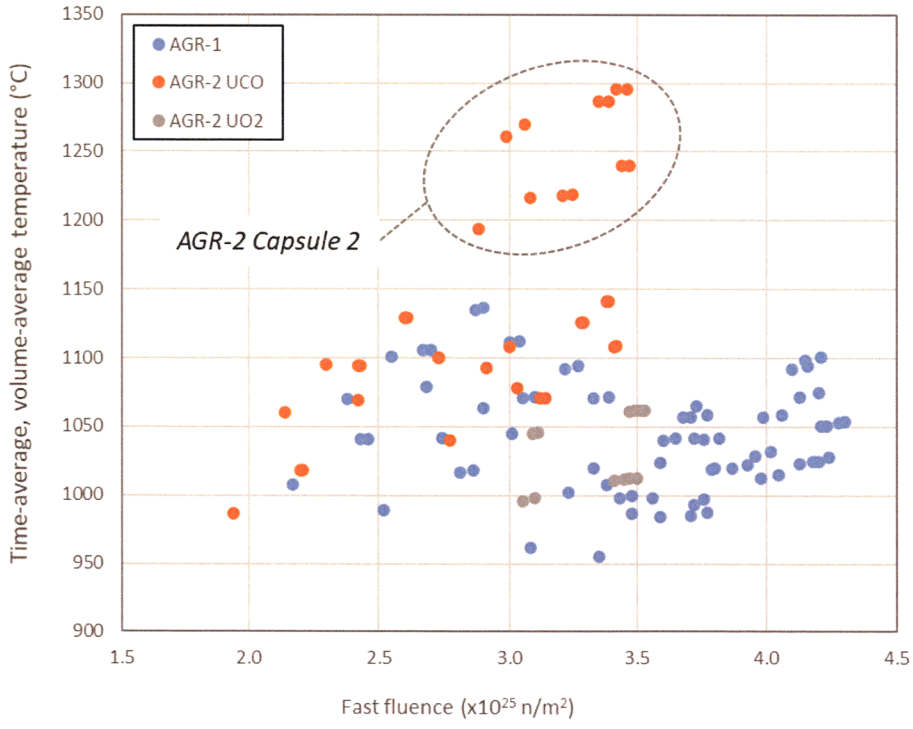

Figure 6-25
AGR-1 and AGR-2 fuel compact TAVA temperatures as a function of fast fluence (E > 0.18 MeV)
Courtesy of Idaho National Laboratory and used with permission of Battelle Energy Alliance, LLC

Further detail on the fuel temperature distributions is provided in Figure 6-26, which presents a cumulative distribution of the duration that fractions of the particle population spent in specific temperature ranges in the AGR-1 irradiation. The data indicate the UCO TRISO fuel was exposed to very high temperatures for long durations, well in excess of those expected in an actual HTGR. Peak time-average temperatures in prismatic HTGRs are usually less than 1250°C. Based on the figure, about 15% of the particle population experienced temperatures in excess of 1250°C for 200 days, 10% of particle population experienced temperatures in excess of 1300°C for 100 days, 5% of particle population experienced temperatures in excess of 1350°C for 50 days, and 2% of particle population experienced temperature in excess of 1400°C for 25 days.

The more severe AGR-1 irradiation conditions compared to the vast majority of historic HTGR designs demonstrate substantial fuel performance margin. Similar plots are provided in Figure 6-27 and Figure 6-28 for AGR-2 where the results from Capsule 2 are separated from Capsules 5 and 6 because it was designed to operate at a time-averaged peak temperature of 1400°C (an early margin test), whereas the other two capsules were designed to be operated at a time-average peak temperature of ≤1250°C.

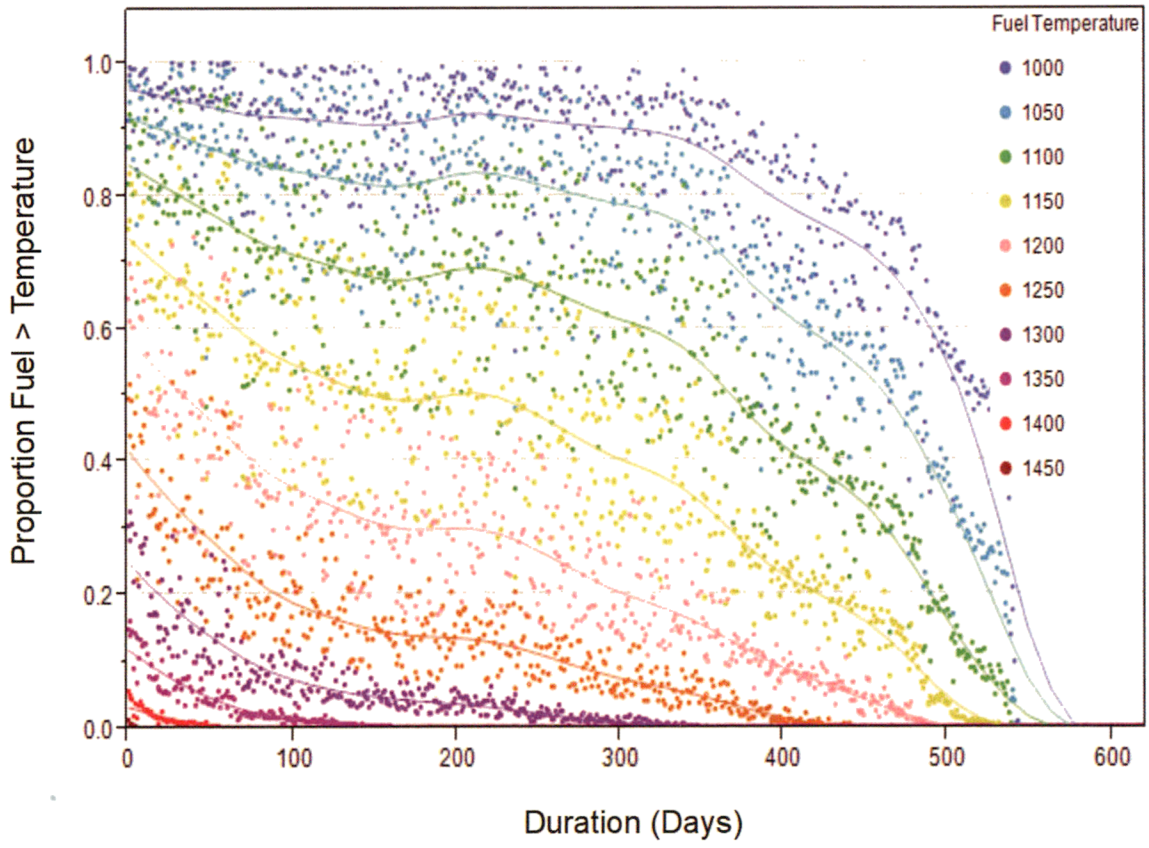

Figure 6-26
Distribution of time at temperature experienced by TRISO fuel particles in AGR-1
Courtesy of Idaho National Laboratory and used with permission of Battelle Energy Alliance, LLC

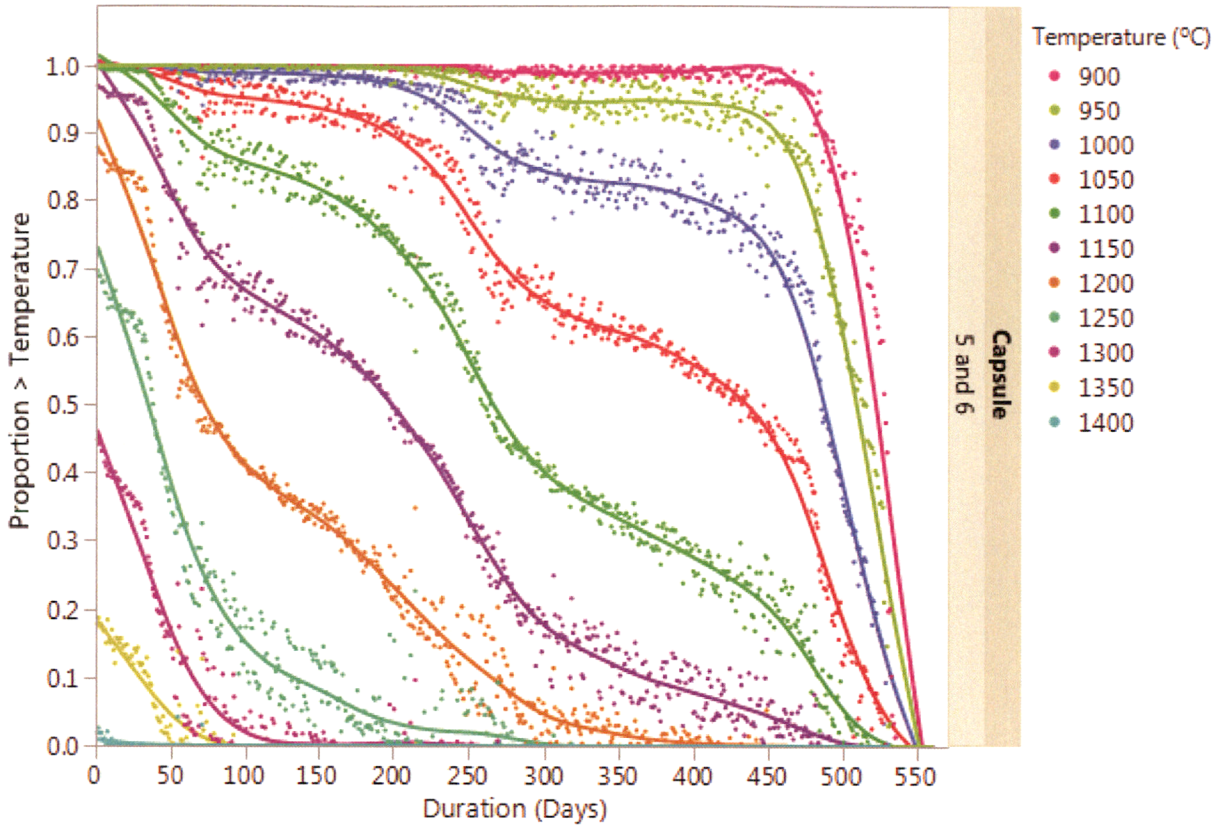

Figure 6-27
Distribution of AGR-2 time at temperature for Capsules 5 and 6 UCO fuel (designed to operate at a time-average temperature of 1250°C)
Courtesy of Idaho National Laboratory and used with permission of Battelle Energy Alliance, LLC

The calculated temperatures in AGR-2 are similar to those in AGR-1 in that much of the fuel operated at high-temperature for significant amounts of time. A key facet of the AGR-2 experiment is the performance results of the UCO in Capsule 2, in which large fractions of the fuel operated at very high temperature (for example, approximately 25% of the particles experienced temperatures in excess of 1400°C for more than 100 days and approximately 10% of the fuel experienced temperatures in excess 1500°C for 30 days).

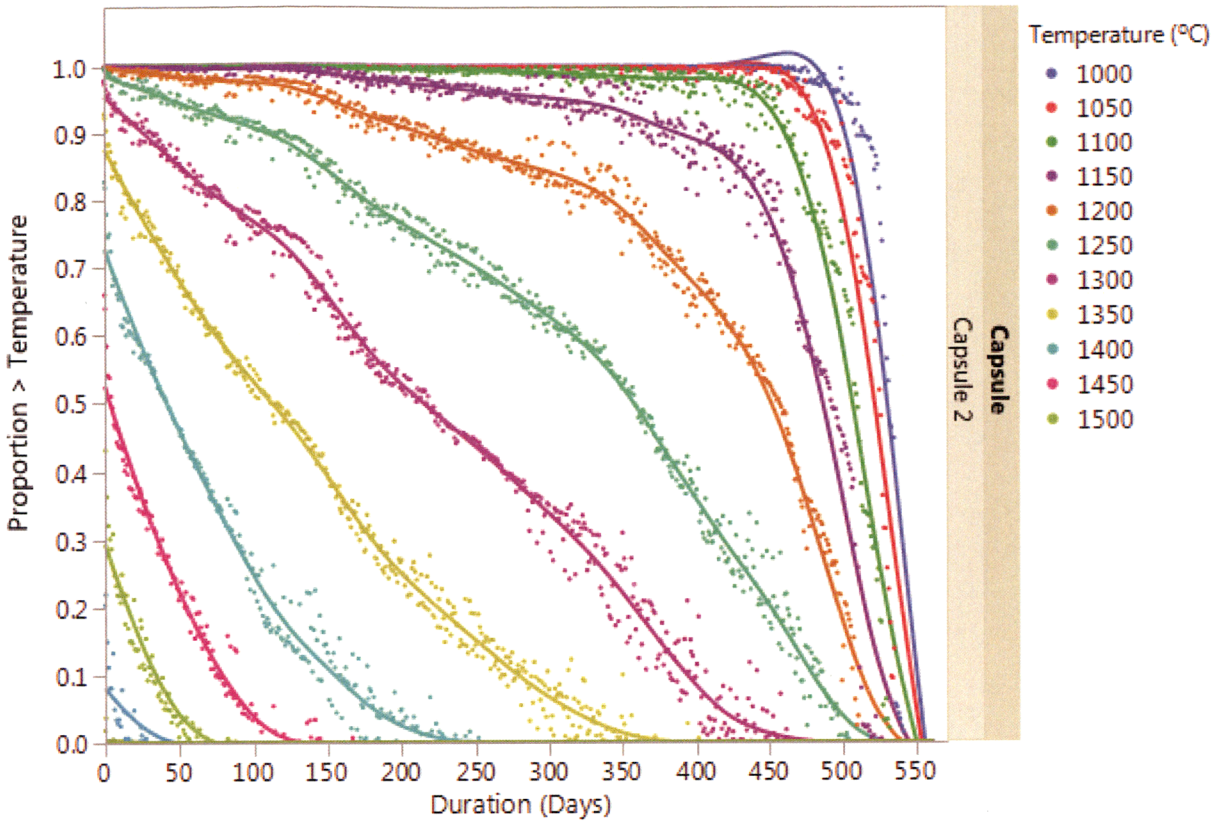

Figure 6-28
Distribution of AGR-2 time at temperature for Capsule 2 UCO fuel (designed to operate at a time-average peak temperature of 1400°C)
Courtesy of Idaho National Laboratory and used with permission of Battelle Energy Alliance, LLC

To provide another perspective of the severity of the AGR irradiations, the temperature distributions from the six capsules in AGR-1 and in Capsules 2, 5, and 6 of AGR-2 (comprising all U.S. UCO fuel) are compared to the distribution calculated for the SC-MHR reactor, a GA MHTGR design with an outlet temperature of 750°C. As can be seen in Figure 6-29, the irradiations are very bounding in terms of temperature relative to that expected in the GA design. The effect would be even more exacerbated in a pebble-bed since the fuel in pebble-bed reactors tends to run cooler than prismatic reactors at the same outlet temperature. These fuel temperatures are significantly higher than expected in FHR designs.

The AGR program recognizes the temperatures in the AGR-1 and AGR-2 irradiations are overly conservative relative to that expected in an operating reactor, but the temperatures were appropriate given the objectives of each experiment: (1) AGR-1 was a proof-of-concept experiment to determine the performance of UCO TRISO-coated particle fuel at the aggressive high-burnup high-temperature conditions proposed for some HTGR designs; and (2) AGR-2 had as its goal to demonstrate the performance of UCO TRISO-coated particle fuel produced in an engineering-scale coater and to perform an early high-temperature margin test.

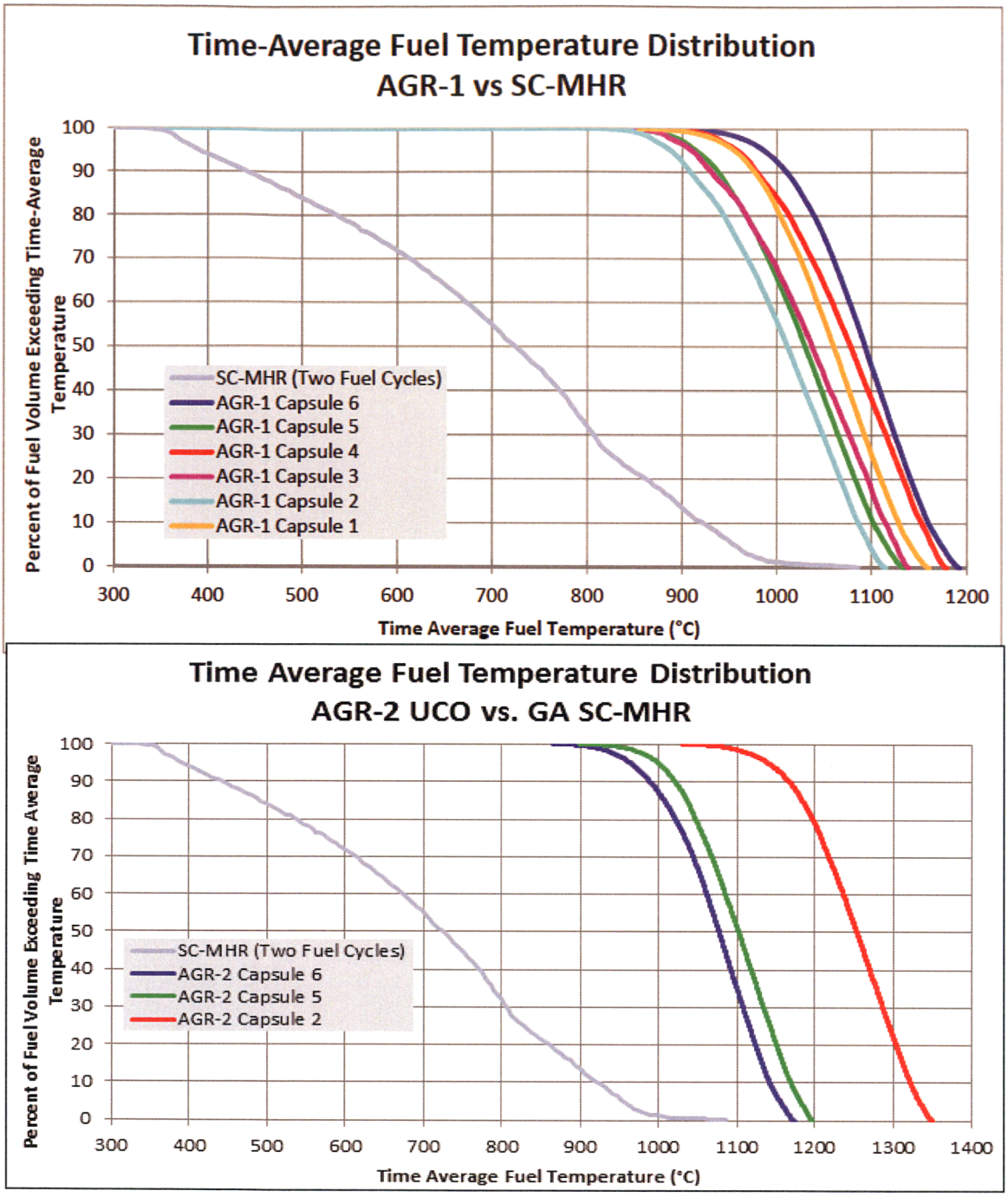

Figure 6-29
Comparison of fuel temperature distribution in AGR-1 and AGR-2 capsules with that expected from a 750°C outlet temperature HTGR (the GA SC-MHR)
Courtesy of Idaho National Laboratory and used with permission of Battelle Energy Alliance, LLC

The key parameters for TRISO fuel performance are burnup, temperature, fast neutron fluence, and power. The ranges of values are summarized in the Table 6-6 and Figure 6-30.

The ranges provided are based on volume averaged values for individual compacts, with the exception of time averaged temperature and particle power. Temperature and power are time averaged over the course of the irradiation. Burnup and fast fluence ranges are based on end-of-life values. Two different sets of parameter ranges have been provided: one data set for all AGR-1 capsules and AGR-2 Capsules 5 and 6, and a separate data set for AGR-2 Capsule 2. This approach has been taken because the AGR-2 Capsule 5 and 6 values predominantly fall within the range for the AGR-1 capsules; the exception is the slightly lower minimum burnup for AGR-2 (7.3% FIMA) compared to AGR-1 (11.1% FIMA). AGR-2 Capsule 2 was irradiated at a significantly higher peak temperature relative to the other capsules, so this population of fuel compacts is considered separately.

Power is provided in two different units in the table. The first represents power density over the entire compact (W/cm^3) and the second is the power per particle (mW/particle). The AGR-1 and AGR-2 particles had kernels with different diameters (350 μm and 427 μm, respectively) so the power per particle values are given for each of these experiments separately in columns 2 and 3 (see Table 6-6 footnotes a and b).

Table 6-6
Ranges of values for key irradiation parameters for AGR-1 and AGR-2 fuel

Property	AGR-1 + AGR-2 Capsules 5 and 6		AGR-2 Capsule 2	
	Max	Min	Max	Min
Burnup (% FIMA)	19.6	7.3	13.2	10.8
Fast fluence ($n/m^2 \times 10^{-25}$; E > 0.18 MeV)	4.30	1.94	3.47	2.88
Time-average temperature (°C)	1210	800	1360	1034
Time-avg compact power density (W/cm^3)	90	50	92	74
Time-avg particle power (mW/particle)	66[a]/86[b]	37[a]/48[b]	88	71

a. AGR-1 values
b. AGR-2 Capsules 5 and 6 values

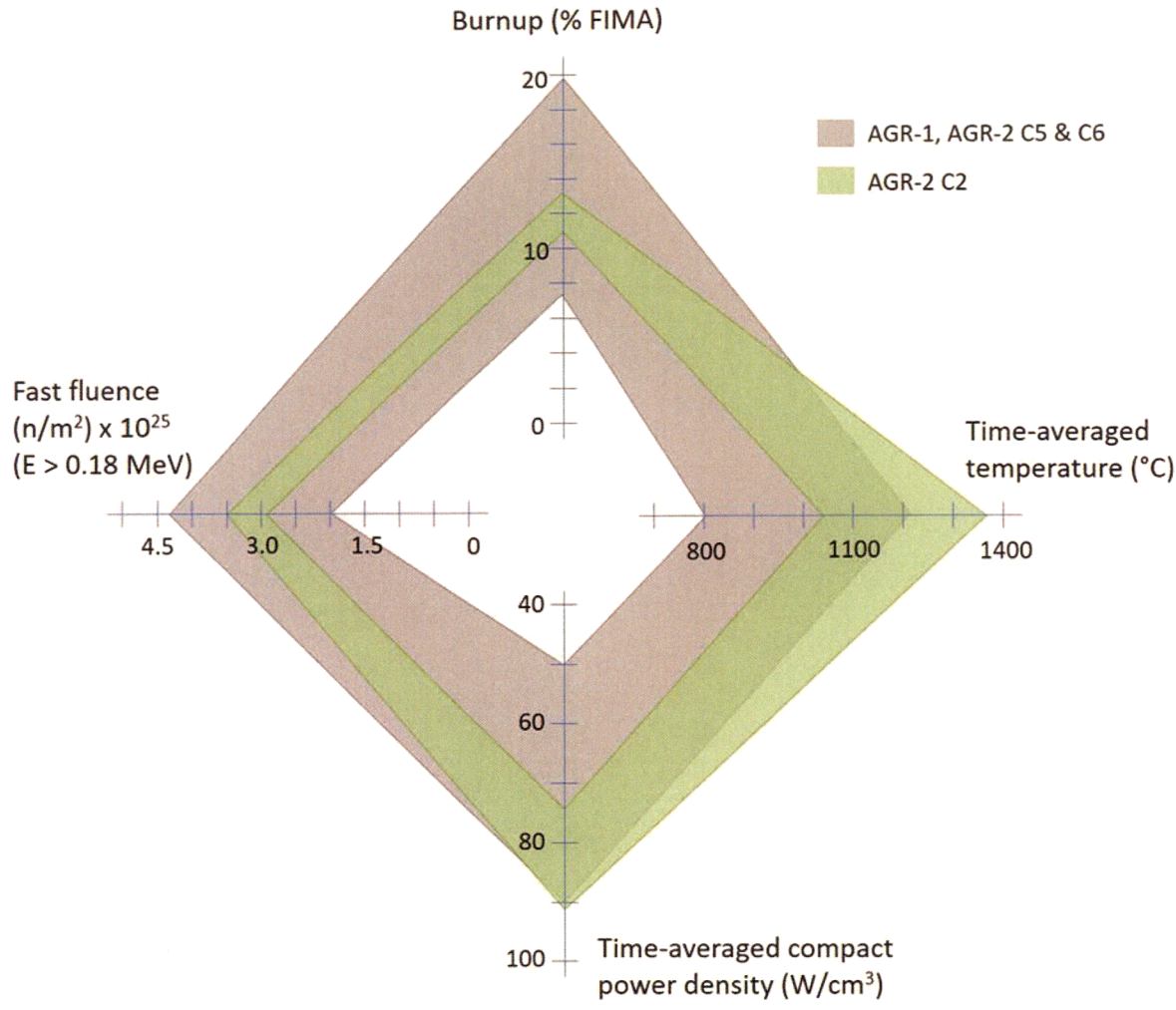

Figure 6-30
Ranges for key irradiation parameters for AGR-1 and AGR-2 fuel

The safety test data presented in the report are for heating in dry helium at temperatures of 1600-1800°C for durations as long as 400 hours. These data generally bound the ranges of conditions typical of past modular high temperature gas reactor designs. Future license applicants will need to justify the applicability of the data to their specific designs.

6.7 Fission Gas Release

The release rate of fission product gases from TRISO fuel particles is a direct method of assessing fuel performance. Fission product R/B ratio values provide indicators of initial fuel quality (that is, level of contamination and as-manufactured exposed fuel kernels) and fuel performance (subsequent TRISO failures) during irradiation. The fission gas isotopes measured by the FPMS during AGR-1 and AGR-2 include ^{85m}Kr, ^{87}Kr, ^{88}Kr, ^{89}Kr, ^{90}Kr, ^{131m}Xe, ^{133}Xe, ^{135}Xe, ^{135m}Xe, ^{137}Xe, ^{138}Xe, and ^{139}Xe. These nuclides were selected for the R/B evaluations because they have relatively short half-lives, allowing each isotope to reach equilibrium concentration in the fuel during each ATR irradiation cycle. The FPMS system described earlier was used to quantify release rates during irradiation giving the R/B ratios for the radionuclides of interest.

The spectrometer detector systems measure the concentrations of various krypton and xenon isotopes in the sweep gas from each capsule. Eight-hour counting intervals are used to measure the isotope concentrations in the sweep gas. The radionuclides of interest decay in transit from the capsule to the counters. Given a certain measured activity, A (μCi), the radionuclide release rate, R (atoms/s), of a particular nuclide can be calculated as:

$$R = 3.7 \times 10^4 \frac{Ae^{\lambda V_T / f}}{\left(1 - e^{-\lambda V_S / f}\right)}$$

Equation 6-1

Where:

V_S is the sample volume (mL)

λ is the nuclide decay constant (s^{-1})

f is the capsule volumetric flow rate (mL/s)

V_T is the transport volume from the capsule to the sample volume (mL).

The transport volumes were determined during a lead-out flow experiment performed at the beginning of each irradiation.

The birth rates of noble gas fission products of interest were calculated using ORIGEN2, Version 2.2. These calculations used compact flux and reaction rates from MCNP. The ORIGEN2 libraries used in the calculation were modified to remove the isotope depletion methods (transmutation and decay) for the isotopes of interest for birthrates. The increase in the concentration of the isotope during the irradiation time interval divided by the irradiation time interval was determined to be the birthrate of the isotope during the time interval. The ratio of the experimentally determined release rates to the calculated birth rates was then computed.

Figure 6-31 shows R/B versus time for ^{85m}Kr, ^{88}Kr, and ^{135}Xe for the AGR-1 irradiation. AGR-1 irradiation cycle numbers are shown across the top of the figure. These are daily average values filtered such that data coinciding with low reactor power or large helium flow rates are removed. The R/B ratios for these nuclides are below approximately 10^{-7} for the duration of the test with the exception of Capsule 5, which reaches higher temperatures during the last two cycles than other capsules and ends the irradiation with an R/B of approximately 2×10^{-7}. (Note: An R/B of 10^{-7} indicates for every 10 million fission gas atoms generated in fission only one is released.)

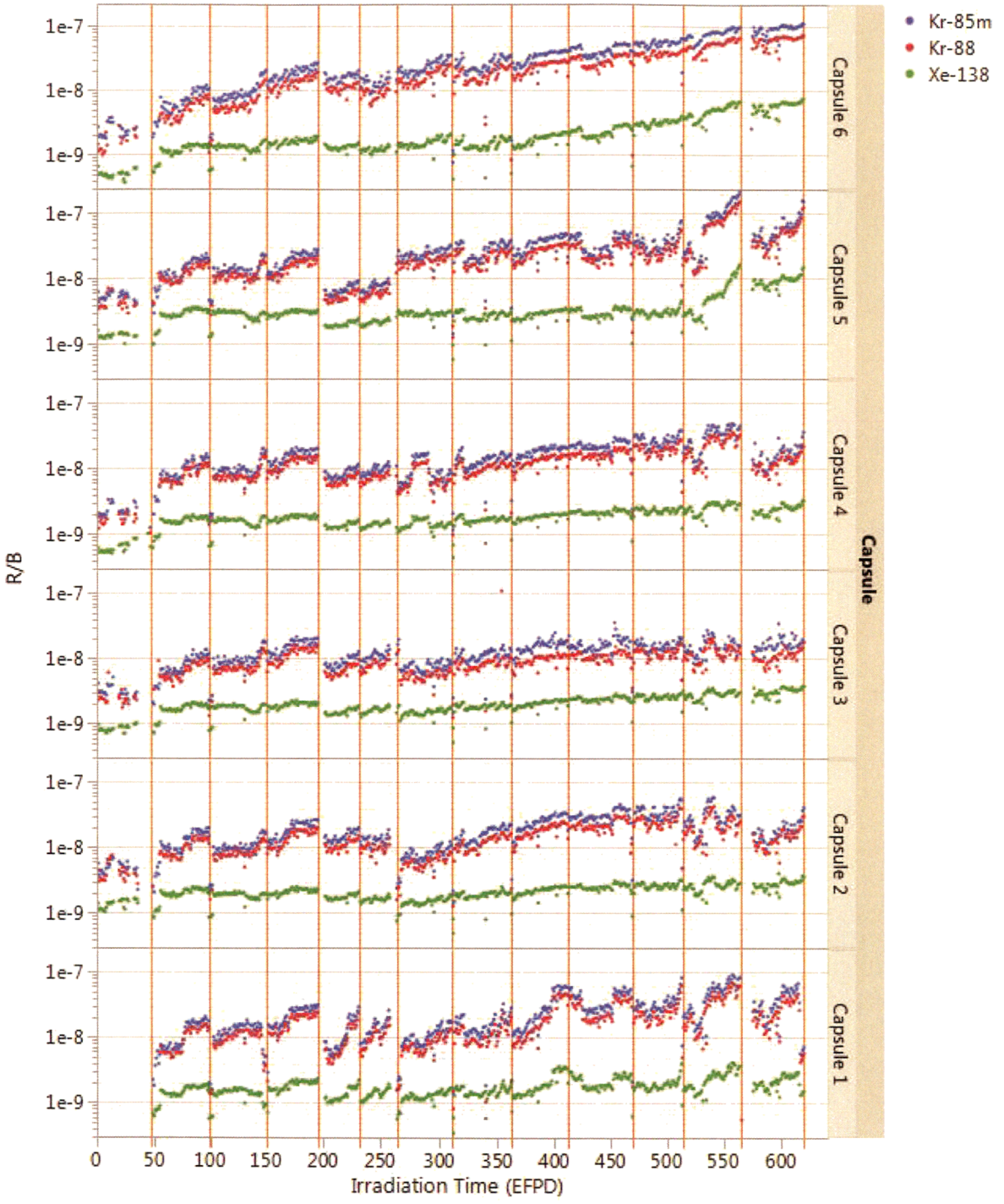

Figure 6-31
AGR-1 R/B ratios for ^{85m}Kr, ^{88}Kr, and ^{135}Xe versus time in EFPDs
Courtesy of Idaho National Laboratory and used with permission of Battelle Energy Alliance, LLC

Figure 6-32 shows R/B versus time for ^{85m}Kr, ^{88}Kr, and ^{138}Xe plotted for AGR-2 for the first three irradiation cycles. Gas flow problems were encountered following test removal from and re-insertion after 150 EFPDs to avoid irradiation during a high-power cycle in ATR. The physical handling of the capsule damaged the refractory gas lines and caused unintentional intermixing of the gas flows between the capsules. As a result, the fission gas data beyond 150 EPPDs (the third irradiation cycle) could not be qualified, and no conclusions about fuel performance beyond Cycle 3 can be drawn based on the R/B data. Accordingly, these data are not shown in Figure 6-32. The capsule gas flows were set to a uniform gas mixture in all capsules until the end of the irradiation so thermal analyses could be performed with a known gas mixture from that point on.

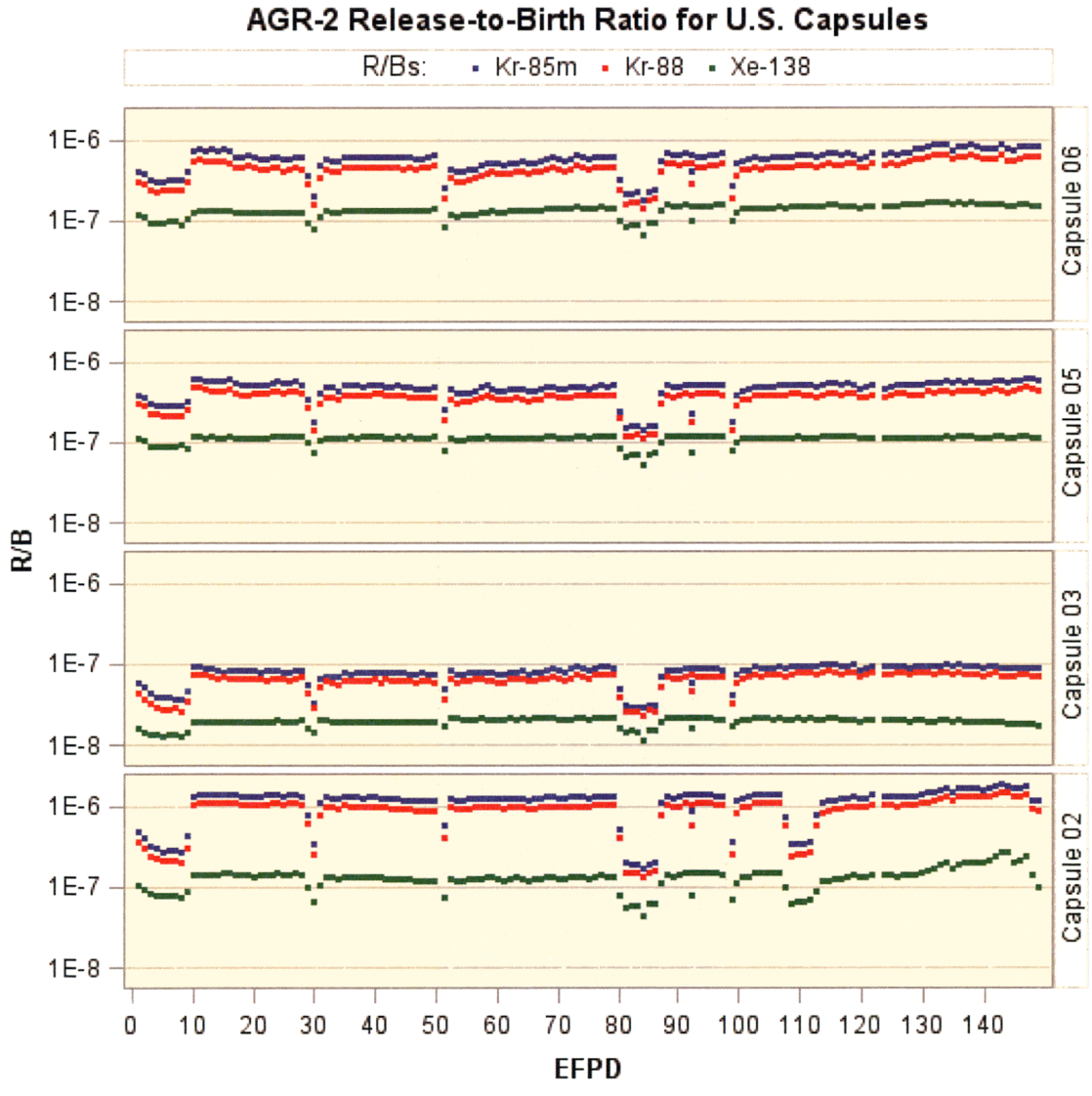

Figure 6-32
AGR-2 R/B ratios for ^{85m}Kr, ^{88}Kr, and ^{138}Xe versus time in EFPDs
Courtesy of Idaho National Laboratory and used with permission of Battelle Energy Alliance, LLC

6.8 Implications on Fuel Performance

AGR-1 end-of-life ^{85m}Kr fission gas release and AGR-2 ^{85m}Kr release through the first three irradiation cycles are compared to historic German and U.S. irradiations in Figure 6-33. The historic data in this figure are taken from the compilation by Petti et al. [66][18]. Mean values for each subset of data are given by the hashmarks and indicate that on average, the R/B results for historic U.S. irradiations were approximately three orders of magnitude higher than the German tests.

The gas release for AGR-1 was extremely low. The UCO fuel in AGR-1 was irradiated to a peak compact-average burnup of 19.6% FIMA, a peak fast neutron fluence of about 4.3×10^{25} n/m^2, and a maximum time-average fuel temperature of approximately 1200°C. About 300,000 TRISO fuel particles were irradiated without a single particle failure, as indicated by the fission-gas measurements on the purge gas from each of the capsules [81]. Thus, AGR-1 is the best irradiation performance of a large quantity of TRISO fuel achieved in the U.S., and the experiments exceeded the German levels of burnup (the reported peak burnup of the German irradiations ranged from 6.9 to 15.6% FIMA, with an average of 10.5% FIMA). These results have confirmed the expected superior irradiation performance of UCO at high burnup in that no kernel migration, no evidence of CO attack of SiC, and no indication of severe SiC attack by noble metal or lanthanide fission products has been observed. Zero fuel failures out of 300,000 particles in the AGR-1 irradiation translates into a 95% confidence failure fraction of $<1.1 \times 10^{-5}$, a factor of 18 better than the prismatic reactor design in-service failure fraction requirement of 2×10^{-4}.

The in-pile R/B results for the first three AGR-2 cycles are shown in Figure 6-32 and summarized in Figure 6-33 [61]. The values are higher than the first several cycles of the AGR-1 irradiation, due in part to higher uranium contamination in the AGR-2 compacts compared to AGR-1 (uranium contamination in the AGR-2 compacts was $\sim 4 \times 10^{-6}$ compared to an average value of 3×10^{-7} for the AGR-1 fuel types). In addition, the mean exposed kernel defect fraction for the AGR-2 fuel was 9.5×10^{-6} ($\leq 2.5 \times 10^{-5}$ at 95% confidence). At this level it is possible to have had an exposed kernel defect in each capsule that would contribute to fission gas release, although the presence of such a defect particle cannot be confirmed based on the R/B data, in part because of the relatively high uranium contamination levels.

No particle failure was observed during the first three cycles of the AGR-2 irradiation. However, because of the cross-talk between capsules due to damage in the gas lines, fission gas release measurements could not be qualified after the third cycle of irradiation. Thus, the possibility of a small number of failures during the later cycles cannot be precluded based on the irradiation data. As a result, the ongoing AGR-2 PIE, which includes an examination of particle failures in the capsules, is being used to help determine the level of particle failure that may have occurred during irradiation.

[18] Reference 66 includes ^{85m}Kr R/B results from eight additional spheres taken from the HFR-K5 and HFR-K6 irradiations. These results are not included in Figure 42, as the end-of-life values are given only as $<3\times10^{-7}$.

The preliminary PIE data currently available indicates at most four particles that experienced TRISO failure in the three UCO capsules using a somewhat conservative approach in identifying particles with failures (discussed in further detail in Section 7.6). Four failures out of 114,000 UCO particles in the experiment corresponds to an actual failure fraction $\leq 8.1 \times 10^{-5}$ at 95% confidence, which is approximately a factor of 2.5 below historic reactor design specification of 2×10^{-4}. In addition, the high-temperature UCO capsule in AGR-2 showed excellent behavior under irradiation, at time-average peak temperature of ≤1360°C, and 25% of the particles in that capsule saw temperatures in excess of 1400°C for over a hundred days. The PIE completed to date has indicated no significant difference in coating failure rates between Capsule 2 and the other two, lower-temperature capsules. This early margin test demonstrated the high-temperature capability of these fuel particles.

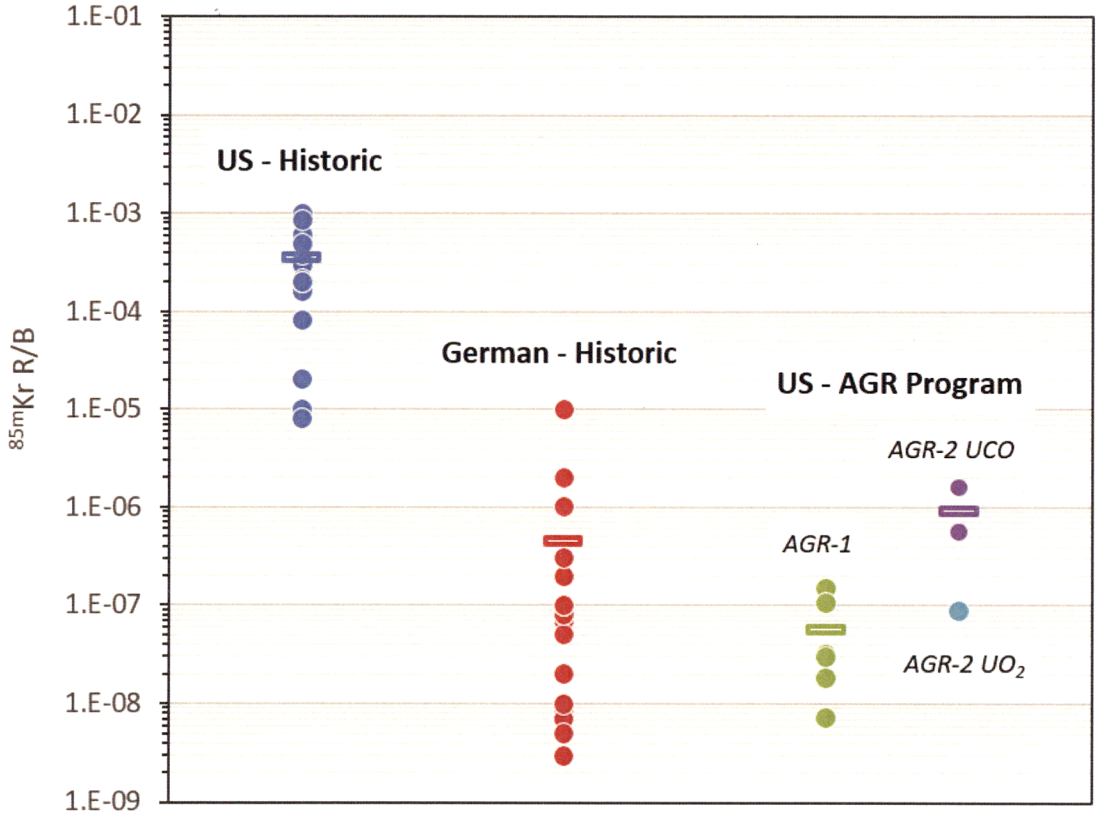

Figure 6-33
^{85m}Kr fission gas release for AGR-1 (end of life) and AGR-2 (after the first three irradiation cycles) compared to historic performance in U.S. and German TRISO fuel irradiations
Courtesy of Idaho National Laboratory and used with permission of Battelle Energy Alliance, LLC

The results from the AGR-1 and AGR-2 irradiations demonstrate excellent performance of UCO TRISO-coated particles that meet historic designer specifications with significant margin. The data confirm the use of the AGR-2 particle as a reference for future high-temperature reactor designs. Beyond the actual performance, it is important to note the fissile kernels of the particles in AGR-1 and AGR-2 were of different size and enrichment, the coatings were applied in coaters of two different sizes (that is, a 2-in. laboratory-scale coater and a 6-in. engineering-scale coater), and further the coating conditions were varied so different microstructures and properties of the coatings were produced.

The excellent behavior with two different UCO kernels confirms the performance of the coatings is the primary factor in achieving good fuel performance and the kernel is of secondary importance. In terms of coating characteristics, AGR-1 particles were fabricated using a range of coating conditions that produced: (1) different combinations of PyC anisotropy and density, which in some cases were intentionally at the edge of the historic specification range; and (2) different microstructures of the SiC—a larger grain, made with traditional hydrogen and MTS coating gases, and a finer grain, by introducing argon gas as a diluent to improve fluidization during SiC deposition.

Based on the in-pile results available at the time, the AGR program decided the AGR-2 PyC coating would be applied using baseline conditions from AGR-1 and would use argon dilution during the SiC coating step, like Variant 3 in AGR-1 for the best fluidization in the coater. Despite these variations in coating conditions, the performance of intact TRISO particles was similar, albeit with slightly higher fission gas release in AGR-2 due to slightly higher uranium contamination of the particle batch in the larger engineering-scale coater and a higher as-fabricated exposed kernel fraction.

The kernels and coatings of the UCO TRISO-coated fuel particles tested in AGR-1 and AGR-2 exhibited property variations and were fabricated under different conditions and at different scales, with remarkably similar excellent irradiation and accident safety performance results. The ranges of those variations in key characteristics of the kernels and coatings are reflected in measured particle layer properties provided in Table 5-5 from AGR-1 and AGR-2. UCO TRISO-coated fuel particles that satisfy the parameter envelope defined by these measured particle layer properties in Table 5-5 can be relied on to provide satisfactory performance.